ANNUAL REVIEWS

Annual Review of Marine Science

Comparing Climate Sensitivity, Past and Present

Eelco J. Rohling,[1,2,*] Gianluca Marino,[1,*] Gavin L. Foster,[2] Philip A. Goodwin,[2] Anna S. von der Heydt,[3] and Peter Köhler[4]

[1]Research School of Earth Sciences, The Australian National University, Canberra 2601, Australia; email: eelco.rohling@anu.edu.au, gianluca.marino@anu.edu.au

[2]Ocean and Earth Science, University of Southampton, Southampton SO14 3ZH, United Kingdom; email: gavin.foster@noc.soton.ac.uk, p.a.goodwin@soton.ac.uk

[3]Institute for Marine and Atmospheric Research Utrecht and Center for Extreme Matter and Emergent Phenomena, Utrecht University, 3584 CC Utrecht, The Netherlands; email: a.s.vonderheydt@uu.nl

[4]Alfred-Wegener-Institut Helmholtz-Zentrum für Polar-und Meeresforschung (AWI), 27515 Bremerhaven, Germany; email: pkoehler@awi.de

Annu. Rev. Mar. Sci. 2018. 10:261–88

First published as a Review in Advance on September 22, 2017

The *Annual Review of Marine Science* is online at marine.annualreviews.org

https://doi.org/10.1146/annurev-marine-121916-063242

*These authors contributed equally to this article

Keywords

climate sensitivity, present climate, paleoclimate, idealized scenarios, feedbacks

Abstract

Climate sensitivity represents the global mean temperature change caused by changes in the radiative balance of climate; it is studied for both present/future (actuo) and past (paleo) climate variations, with the former based on instrumental records and/or various types of model simulations. Paleo-estimates are often considered informative for assessments of actuo-climate change caused by anthropogenic greenhouse forcing, but this utility remains debated because of concerns about the impacts of uncertainties, assumptions, and incomplete knowledge about controlling mechanisms in the dynamic climate system, with its multiple interacting feedbacks and their potential dependence on the climate background state. This is exacerbated by the need to assess actuo- and paleoclimate sensitivity over different timescales, with different drivers, and with different (data and/or model) limitations. Here, we visualize these impacts with idealized representations that graphically illustrate the nature of time-dependent actuo- and paleoclimate sensitivity estimates, evaluating the strengths, weaknesses, agreements, and differences of the two approaches. We also highlight priorities for future research to improve the use of paleo-estimates in evaluations of current climate change.

1. INTRODUCTION

Studies of past and future climate change often center on some climate sensitivity to changes in the radiative balance of the Earth. This sensitivity appears in many guises. The equilibrium climate sensitivity (ECS) is the equilibrium global annual mean temperature rise caused by a doubling of atmospheric CO_2 concentration (Charney et al. 1979, Knutti & Hegerl 2008, IPCC 2013, Forster 2016, Stevens et al. 2016) or a radiative forcing of approximately 3.7 W m^{-2} (Myhre et al. 1998, Byrne & Goldblatt 2014, Etminan et al. 2016), which can be further amplified or dampened by several feedbacks within the climate system acting on many different timescales (e.g., von der Heydt et al. 2016). The amount of global annual mean temperature change in response to a given change in Earth's radiative balance is called either the climate sensitivity parameter or the specific climate sensitivity (in K W^{-1} m^2 or °C W^{-1} m^2). The transient climate response is the global annual mean temperature rise at the time of CO_2 doubling, which arises from a linear increase (1% y^{-1}) in CO_2 forcing over a period of 70 years (IPCC 2013).

Regardless of which definition or timescale is considered, the response (or sensitivity) of climate (or temperature) to a perturbation in the radiative balance (or forcing) is an important metric for evaluating the potential outcomes of anthropogenic impacts on the radiative balance, such as greenhouse-gas releases, land-use changes, and aerosol emissions. The radiative balance, in turn, represents the sum of radiative forcings and feedbacks (where the latter occur over a wide range of timescales) (**Figure 1**), which collectively determine the surface temperature on Earth. Feedbacks are commonly categorized as fast (when acting within less than 100 years) or slow (when acting over longer timescales), although this timescale-based distinction is somewhat blurry in reality (see overview in PALAEOSENS 2012) (**Figure 1**).

Attempts at constraining climate sensitivity have been made throughout the past century and earlier, and despite advances in our understanding of the physical processes that govern Earth's climate, the estimates have not changed much from the very earliest ones (Arrhenius 1896, Callendar 1938, IPCC 2013, Stevens et al. 2016). Current estimates of climate sensitivity remain within a 66% probability range of 1.5–4.5 K (Charney et al. 1979, IPCC 2013, Stevens et al. 2016). But research into this climate metric has intensified in recent years, notably because of increasing concerns about our future global warming trajectory and implementation of mitigation strategies (Mann 2014). Climate sensitivity has been extensively investigated in studies that link observations and modeling both for past (paleo) climates (e.g., Lunt et al. 2010) and for the modern climate with projections into the future (e.g., Fasullo & Trenberth 2012, Sherwood et al. 2014). Another intensive branch of research estimates climate sensitivity directly from paleoclimate reconstructions (Hansen & Sato 2012, PALAEOSENS 2012, Skinner 2012, Royer 2016, von der Heydt et al. 2016). An emerging property of recent investigations into present-day ECS is some apparent nonlinearity or climate-background-state dependence (Knutti & Rugenstein 2015). In the typical approach to calculating ECS—extrapolating transient climate simulations following an abrupt doubling of CO_2 (i.e., $2 \times CO_2$) to the point when the surface temperature change becomes zero—it turns out that a linear relationship is not the best approximation (Bloch-Johnson et al. 2015) and that the so-called fast feedbacks are still changing after more than 150 years (Rugenstein et al. 2016b). These are key issues for further research. In addition, there is interest in better understanding climate sensitivity and the forcing and feedback processes that control Earth's climate through past episodes of climate change, such as the Plio-Pleistocene glacial-interglacial cycles and earlier Cenozoic events and sustained episodes of global warming. In this field, potential state dependence is also a key focus.

Paleoclimate data can be used to evaluate climate sensitivity in several ways, including (*a*) analyzing time series of the recent past, such as the last millennium (Hegerl et al. 2006);

(*b*) comparing the present (preindustrial) with specific time slices, such as the Last Glacial Maximum (Hansen et al. 1984, Schneider von Deimling et al. 2006, Schmittner et al. 2011) or Cenozoic intervals that were warmer and had higher-than-preindustrial atmospheric CO_2 concentrations (Pagani et al. 2010, Hansen et al. 2013b, Anagnostou et al. 2016); and (*c*) studying multiple climate cycles, such as the repeated alternation between glacial and interglacial periods that characterized the Pleistocene (Hansen et al. 2007, Rohling et al. 2012, von der Heydt et al. 2014, Köhler et al. 2015, Friedrich et al. 2016) and the Pliocene (Martínez-Botí et al. 2015). These approaches suffer from relatively large uncertainties that are inherent to the use of proxy data, owing to a shortage of globally distributed data sets of past temperature changes that span the desired timescales and from problems in obtaining consistent chronologies for the various time series of climate forcing and responses. Regardless, climate sensitivity estimates from paleoclimate data have the merits of being based on real data, thus including all known and unknown feedbacks, and being calculated through a full range of climate states, including those colder and warmer than the preindustrial state.

Climate sensitivity to changes in climate forcing depends on numerous response (feedback) processes—all with their own (uncertain) timescales (**Figure 1**) and (uncertain) relative radiative contributions, or efficacies (Hansen et al. 2005, Bony et al. 2006). The conceptual background has

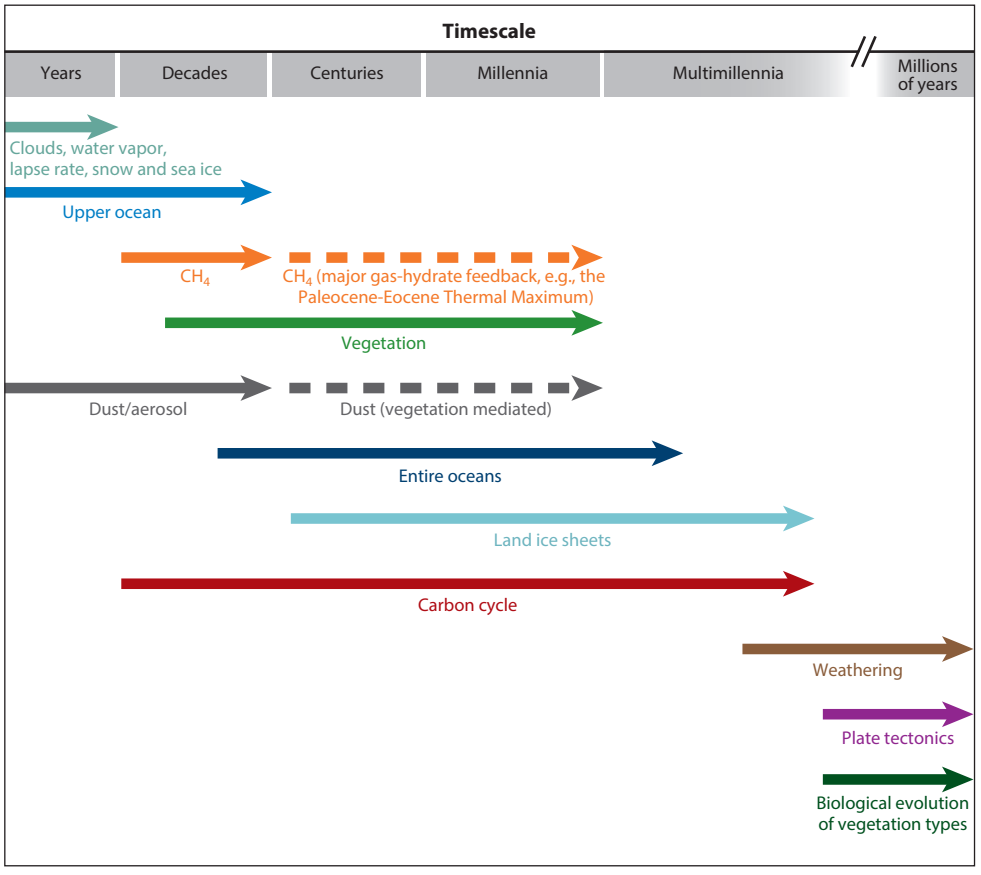

Figure 1

Timescales of processes involved in climate sensitivity. Based on a synthesis in PALAEOSENS (2012).

been previously discussed in relation to both modern/future (actuo) climate change and paleoclimate change (e.g., Charney et al. 1979; Hansen et al. 1984, 2005, 2007, 2008, 2013b; Skinner 2012; Marvel et al. 2016; von der Heydt et al. 2016). PALAEOSENS (2012) synthesized discussions and mathematically evaluated relationships.

Here, we outline the PALAEOSENS (2012) framework and consider its implications and challenges. We then formulate some simple, purely theoretical, graphical representations to illustrate and evaluate the nature of the probability distributions for climate sensitivity in response to anthropogenic forcing and through episodes of climate change in the paleoclimate record. We use these schematic representations to investigate how climate sensitivities from actuo- and paleo-studies can best be assessed to make them comparable to one another. Finally, we consider implications of the results for the potential of narrowing down the climate sensitivity range and/or its dependence on climate background states.

2. FRAMEWORK

PALAEOSENS (2012) outlined an approach that uses reconstructions of key climate parameters in the geological past to approximate the equilibrium fast-feedback climate sensitivity term that applies to actuo-climate studies (S^a, i.e., the ECS calculated when all fast feedbacks and surface-ocean warming have completed). The main issue that needed to be addressed in aligning climate sensitivity estimates from paleoclimate studies with those from actuo-climate studies concerns the contrasting timescales involved—natural climate change is much slower than anthropogenic climate change (Crowley 1990, Zeebe et al. 2016). Natural change therefore includes the action of feedbacks that are too slow to be relevant over the next 100–200 years and/or relate to processes that are not (yet) included in climate models owing to computational limits (e.g., continental ice sheets).

One way to address this issue uses the so-called time-dependent climate sensitivity approach, which accounts for both fast and slow feedbacks and allows evaluation of climate sensitivity continuously over timescales that are relevant to both the imminent future and the distant geologic past (Zeebe 2013). It builds on the notion that fast and slow feedbacks operate continuously in the climate system, thereby modulating the evolution of climate and its sensitivity to forcing through time. In this time-dependent climate sensitivity approach, the fast-feedback climate sensitivity is set (to 3 K), whereas the evolution of the slow feedbacks (carbon cycle, vegetation, low-latitude glaciers, and polar ice sheets) is modeled using constraints from the paleoclimate record. The strength of this approach for future climate projections lies in the comprehensive estimates of anthropogenic warming (and its duration) that it delivers. For example, it accounts for the impacts of warming on the solubility of CO_2 in the ocean, which further enhance global warming by increasing atmospheric CO_2 concentrations (Zeebe 2013). Note that this approach relies on a linearization of the climate response around the background climate and applies only to cases where the climate system (after a very long time) reaches a unique and true equilibrium. In reality, the climate system may instead (*a*) exhibit variability on many different timescales (interannual to orbital), with potentially different characteristics under CO_2 forcing, and (*b*) cross tipping points that imply highly nonlinear climate responses (e.g., Drijfhout et al. 2015).

Another approach, which has been more extensively applied, explicitly resolves radiative forcing caused by the slow-feedback processes (e.g., ice-sheet albedo, vegetation albedo, and/or greenhouse-gas concentrations) and then removes their influences from the calculated climate sensitivity (Hansen et al. 2007, Köhler et al. 2010, Masson-Delmotte et al. 2010, PALAEOSENS 2012, Rohling et al. 2012, Martínez-Botí et al. 2015). PALAEOSENS (2012) proposed the parameter S^p for paleoclimate sensitivity in terms of temperature change relative to forcing resulting

only from CO_2 change, which is equivalent to their specific climate sensitivity term $S_{[CO2]}$ [also named Earth system sensitivity (ESS) by Lunt et al. (2010)]. Similar specific climate sensitivity terms can be formulated relative to other (combinations of) slow-feedback processes, e.g., relative to changes in CO_2 and land ice ($S_{[CO2,LI]}$) or to changes in overall greenhouse-gas levels, land-ice albedo, and vegetation albedo ($S_{[GHG,LI,VG]}$). Conceptually, the PALAEOSENS (2012) approach assumes that S^p can be "corrected" for all processes that are either slow (conventionally taken to mean acting over more than 100 years) or not included in models, such that one ends up with an approximation of S^a. The subscripts then identify the slow feedbacks that are corrected for—or, in other words, those that are effectively considered to be climate forcings. This is a pragmatic approach that requires knowledge about the radiative impacts of all processes at any moment in the past, which then becomes the real challenge. Here, we evaluate the comparability between actuo and paleo examples, following the PALAEOSENS (2012) approach of focusing on specific radiative contributions of the various processes, because this approach can be illustrated relatively easily in graphical examples.

In more specific terms, PALAEOSENS (2012) argued that the observed relatively low rates of temperature change imply that the climate remained close to equilibrium in the preindustrial past. In general, global annual mean temperature changes are small relative to the 288 K (15°C) absolute temperature of Earth's surface. Temperature change (warming) over the past several decades amounts to between 0.01 K y^{-1} (IPCC 2013) and 0.015 K y^{-1} (Hansen et al. 2010). During Pleistocene deglaciations, it was an order of magnitude slower (Masson-Delmotte et al. 2010, Shakun et al. 2012, Friedrich et al. 2016, Snyder 2016), and during the dramatic onset of the Paleocene-Eocene Thermal Maximum, 56 Mya, rates of global warming were somewhere between those two values (Zachos et al. 2006, Zeebe et al. 2009, Kemp et al. 2015). Today, climate is affected by an external forcing (notably greenhouse-gas release) that is increasing faster than all but the fastest climate processes can respond. Thus, the climate remains in a state of disequilibrium until sufficient time has elapsed for the slower processes to adjust, where completion of centennial-scale surface-ocean heat uptake is commonly used to denote equilibrium. Indeed, the energy imbalance caused by ocean heat uptake is widely used as a measure of the overall disequilibrium state (e.g., Hansen et al. 2011, 2013a,b, 2017). During most of the preindustrial past, climate feedbacks were close to equilibrium with the global temperature, given that these processes themselves were driving the climate changes.

For close-to-equilibrium changes in the past, the radiative impacts of the global mean external climate forcings (negligible annual mean global insolation changes), slow feedbacks (including carbon-cycle processes), and fast feedbacks must have been almost, if not precisely, balanced. Hence, $\Delta R_{[sf]} + \Delta R_{[ff]} \approx 0$, where ΔR stands for radiative change, "sf" stands for the sum of all (slow-feedback) forcings, and "ff" stands for the sum of fast feedbacks (for more detail, see PALAEOSENS 2012, von der Heydt et al. 2014, von der Heydt & Ashwin 2016). Thus, for a given (small) temperature change, ΔT, the equilibrium fast-feedback climate sensitivity parameter $S^a = \Delta T / \Delta R_{[ff]}$ may be approximated by $S_{[sf]} = \Delta T / \Delta R_{[sf]}$. Estimates following this approach throughout the Cenozoic consistently fall within a distribution of approximately 0.3–1.9 or 0.6–1.3 K W^{-1} m^2 at 95% or 68% probability, respectively (Köhler et al. 2010, Masson-Delmotte et al. 2011, PALAEOSENS 2012, Rohling et al. 2012, Martínez-Botí et al. 2015, Anagnostou et al. 2016, Friedrich et al. 2016). The latter scales to a warming of 2.2–4.8 K per doubling of atmospheric CO_2 concentrations, in agreement with IPCC (2013) estimates.

A major question that remains open is whether this distribution reflects (*a*) reconstructed climate sensitivity values that are scattered randomly through the range that is determined (i.e., random uncertainty) or (*b*) more likely, a combination of different, narrower paleoclimate sensitivity ranges from different time periods, and in particular from different climate background states,

which would therefore represent a systematic source of uncertainty (see also Stevens et al. 2016, von der Heydt et al. 2016). Indeed, model-based process studies and theoretical considerations drive an expectation that the value of climate sensitivity should depend on the prevailing climate background state, because contributing feedback processes may become more or less effective (i.e., their efficacies may change) under different background climate conditions (for attempts to define different types of state dependence, see, e.g., Crucifix 2006, von der Heydt et al. 2016). Recent work (von der Heydt et al. 2014, 2016; Köhler et al. 2015) suggests that state dependence may be detectable with model-based interpretation of the data, but the matter has not been conclusively resolved owing to uncertainties involved in the data and the (chronological) comparisons between records. In detail, the state dependence identified by Köhler et al. (2015) resulted mainly from calculation of the land-ice albedo radiative forcing, $\Delta R_{[LI]}$, based on deconvolution of the global deep-sea benthic oxygen isotope record with three-dimensional ice-sheet models. Another, relatively minor contribution resulted from the latitudinal dependence of changes in incoming insolation, *I*. Combined, these drove a nonlinear relationship between $\Delta R_{[LI]}$ and sea level. Earlier approaches used simpler one-dimensional ice-sheet models (van de Wal et al. 2011), did not similarly account for the latitudinal dependence of *I* (Köhler et al. 2010, PALAEOSENS 2012), or approximated $\Delta R_{[LI]}$ as a linear function of sea level (Hansen et al. 2008, Martínez-Botí et al. 2015) and therefore were primed to miss the state dependence detected by Köhler et al. (2015). More recently, Friedrich et al. (2016) found a similar state-dependent, nonlinear relationship between global temperature and radiative forcing anomalies over the last 784,000 years. Briefly, they determined global annual mean temperature variations using a combination of proxy reconstructions from marine sediment cores and simulation results from an Earth system model of intermediate complexity. The latter was also used to characterize the planetary albedo through the last 784,000 years by simulating the radiative impacts of ice sheets, continental shelf inundation/exposure, and vegetation cover. The greenhouse-gas forcing was quantified from ice-core records. Finally, Friedrich et al. (2016) detected climate sensitivity and its state dependence from the local slope of the temperature versus radiative forcing regression, similar to previous studies (e.g., Köhler et al. 2015).

A key cause of state dependence of climate sensitivity—especially with respect to slow feedbacks—concerns changes in the efficacy of one or more of these feedbacks under different climate states, meaning that the radiative contribution of these processes changes through time. For example, a similar unit area of ice has a stronger radiative impact at lower latitudes than at higher latitudes owing to greater amounts of incoming radiation per unit area as the equator is approached; i.e., the efficacy of the ice albedo feedback may be noticeably stronger for lower-latitude ice than for higher-latitude ice. This notion has implications for paleoclimate sensitivity studies that consider both maximum and intermediate glaciation states. In another example, large-scale clustering of continental mass at low latitudes in the Neoproterozoic supercontinent of Rodinia is thought to have amplified the difference between continental reflection and sea-surface absorption of incoming solar radiation relative to distributions with more continental mass at higher latitudes, which facilitated major global cooling that eventually led to Snowball Earth (Kirschvink 1992), although this influence remains contested (Poulsen et al. 2002). State dependence of climate sensitivity may also result from less obvious changes that—in particular for fast feedbacks—are not necessarily well approximated in terms of efficacy changes. Among these, variations in cloud coverage and types are among the least understood parameters in paleoclimate studies, even though they likely exerted a major control on both albedo and retention of outgoing long-wave radiation (e.g., Bony et al. 2015, Zhou et al. 2016).

So far, it is virtually impossible to develop a comprehensive view of past efficacy changes for most feedbacks, which complicates the reconstruction of state dependence in paleodata-based

studies. A pragmatic solution is therefore needed. One approach assumes constant efficacies for all feedbacks and then assesses whether calculated ECSs appear to have been constant or variable with climate background state. Any inferred variations subsequently become targets for investigating the potential variability of feedback efficacies. Alternatively, hybrid approaches are possible, in which feedback efficacies through time are assessed with climate models. But this technique introduces potential model bias into the primarily observation-based estimates, meaning that subsequent comparisons with model-based results become somewhat circular.

In the next section, we use highly idealized examples to graphically illustrate (*a*) the controls on paleoclimate sensitivity probability distributions, (*b*) the limitations resulting from data availability issues that affect approximations of S^{a} using $S_{[sf]}$ in paleodata-based studies, and (*c*) how state dependence caused by temporal changes in feedback efficacy may factor into the reconstructed probability distributions.

3. ACTUO-CLIMATE VERSUS PALEOCLIMATE SENSITIVITY

As a first step toward more precise assessments of climate sensitivity, PALAEOSENS (2012) advocated strict adherence to specific definitions to avoid conflating information that applies over different timescales and different climate background states, as tends to occur in broadly generalized approaches (Pagani et al. 2010, Snyder 2016). However, although the PALAEOSENS (2012) framework may ensure like-for-like comparisons, it still involves choices and assumptions that may affect the outcome (e.g., Skinner 2012). As a consequence, climate sensitivity is more a moving target than a unique fixed number, depending on the choices and assumptions made and the timescales and climate background states over which it is considered. In addition, from the point of view of dynamical systems theory, climate sensitivity is more likely a probability distribution than a single number (von der Heydt & Ashwin 2016), where the distribution arises not from randomness or observational errors but from the actual climate-system dynamics that exhibit state-dependent behavior through their fast-feedback processes. Thus, pertinent questions remain about the extent to which a determination of $S_{[sf]}$ may provide insight into the S^{a} that is relevant to anthropogenic forcing. We explore this with simple, schematic, idealized graphic example scenarios.

In contrast to most modeling approaches to climate sensitivity, we consider here a time-dependent climate sensitivity $S(t)$ to reflect both the short-term variations and longer-term background-state dependence of S. We follow the general principles laid out above (PALAEOSENS 2012), where S is determined by the radiative balance of the planet and different feedbacks enhance or dampen the initial temperature response:

$$S = \frac{\Delta T}{\Delta R} = \frac{-1}{\lambda_{\mathrm{P}} + \sum_{i=1}^{N} \lambda_i^{\mathrm{f}} + \sum_{j=1}^{M} \lambda_j^{\mathrm{s}}}. \qquad 1.$$

Here, the λ terms refer to the strength of different feedback processes (in terms of a feedback factor, in W m^{-2} K^{-1}), sorted by the timescale on which they act: λ_{P} reflects the change in long-wave radiation in the absence of other feedbacks (the so-called Planck feedback), and the superscripts "f" and "s" denote N fast-feedback and M slow-feedback processes, respectively. Note that Equation 1 includes the sum of slow feedbacks (the third term in the denominator), which is the version applicable for calculating paleoclimate sensitivity in the PALAEOSENS (2012) framework. For actuo-climate sensitivity, that sum of slow feedbacks is omitted from the denominator.

Generally, feedback factors are assumed to be constant. However, to reflect the state dependence of feedbacks, a time-dependent climate sensitivity, $S(t)$, results from the fact that both λ^{f} and λ^{s} can be time dependent. For example, the state dependence of fast-feedback processes as

inferred between glacial and interglacial periods (von der Heydt et al. 2014) may be represented by a (long-timescale) variation of $\lambda^f(t)$. The different response times in all feedback factors can be reflected by a delayed growth of the feedback factors for those processes with slower timescales. The first details in this direction were published by Zeebe (2013), who assumed that the slow-feedback processes, λ^s, grow from zero to their full strength after a certain time delay.

We adopt a similar approach, with a focus on changes in the time domain. However, our schematic scenarios build up the argument in terms of simple prescribed functions for the radiative contributions (ΔR) from the various processes, rather than in terms of feedback responses. We did this because we aim to graphically compare actuo- and paleo-scenarios, and for paleo-scenarios the data more directly resolve ΔR contributions (Hansen et al. 2007, 2008; Köhler et al. 2010; Masson-Delmotte et al. 2010; Rohling et al. 2012).

Our actuo-scenario (Section 3.1) and paleo-scenario (Section 3.2) represent processes that control changes in the radiative balance of climate by means of simple prescribed sigmoidal response functions, with random, uniformly distributed uncertainty ranges that are evaluated in a Monte Carlo–style approach of 1,000 separate instances. Each response function describes a schematic time-dependent development of a radiative anomaly, in which a phase of exponentially increasing growth from zero is followed (in a symmetrical manner through time) by a phase of exponentially decreasing growth before settling at the stipulated maximum radiative impact of the process considered. The various response functions are then summed up, giving a median record of total radiative change over time and an uncertainty range based on percentile ranges across all Monte Carlo instances. A rough scaling is worked out for each instance to calibrate the record of total radiative change to one of total temperature change over time. This temperature record is then used in a ratio relative to the records for component sums $\Delta R_{[ff]}$ and $\Delta R_{[sf]}$ to estimate the implied S^a and $S_{[sf]}$, respectively.

Although our radiative response functions are simple prescribed functions rather than fully interactive feedback processes, we aim to use reasonably realistic amplitude scalings (efficacies) for the contributing radiative (feedback) processes in both the actuo- and paleo-scenarios, based on published numbers for the modern climate and for Pleistocene glacial-interglacial cycles. We emphasize that the scenarios may not be viewed as in-depth analyses because they do not comprehensively represent the interactive physics of the climate system. Including the latter would deeply entangle the idealized results shown here and confound relationships between the various climate sensitivity definitions and their underlying processes, which would make it more difficult to visualize the potential impacts of issues such as limited data availability, unknown past processes, and fundamental uncertainties. Our idealized example scenarios guide the discussion by visualizing such impacts (Sections 4.1 and 4.2). Finally, given that our approach—which draws on proxy-based paleo-reconstructions of radiative forcing anomalies (ΔR) to calculate temperature change (ΔT) and climate sensitivity (S)—may be less familiar to climate modelers, we end the discussion with an illustration of how the importance of the time domain might be addressed in a feedback-focused analysis framework (Section 4.3).

3.1. Illustrative Scenario for Actuo-Climate Sensitivity

For the actuo-climate scenario, we consider that, for any given trigger (e.g., greenhouse-gas emissions), a sequence develops of delayed temperature responses (indicated with δ) and radiative feedback responses (indicated with ΔR), all with their own timescales and amplitudes (**Table 1**). Key responses to be taken into account are the direct warming effect of the emissions, the associated outgoing long-wave radiation cooling response (Planck response), and other typical very fast feedbacks, which include changes in water-vapor content, atmospheric lapse rate, and

Table 1 Parameter values used in our idealized actuo-climate sensitivity scenario

Description	Code	Estimated duration for full response (τ) (years)	Full range (ε_τ, uniform distribution)	Full amplitude (b) (W m^{-2})[a]	Full range (ε_b, uniform distribution)
Direct responses, including vapor and cloud feedbacks	$\Delta R_{[T2]}$	1	±50%	2.2	±10%
Aerosol and land-surface feedbacks	$\Delta R_{[AE]}$	10	±50%	−1.2	±50%
Snow and sea-ice albedo feedback	$\Delta R_{[SSI]}$	20	±50%	0.4	±10%
Carbon-cycle feedbacks	$\Delta R_{[CFB]}$	150	±50%	$0.05 \times \Delta R_{[T2]}$	±50%
Surface-ocean temperature equilibration	$\delta_{[SO]}$	150	±50%	0.55	±10%
Continental ice albedo feedback	$\Delta R_{[LI]}$	750	±50%	$3 \times (10/125)$	±50%
Deep-ocean temperature equilibration	$\delta_{[DO]}$	1,500	±50%	0.55	±10%
Vegetation albedo	$\Delta R_{[VG]}$	500	±50%	$0.05 \times (\Delta R_{[AE]} + \Delta R_{[T2]})$	±50%
Carbonate compensation	$\Delta R_{[CC]}$	10,000	±50%	$-0.5 \times (\Delta R_{[CFB]} + 0.5 \times \Delta R_{[T2]})$	±50%
Weathering	$\Delta R_{[WE]}$	200,000[b]	±50%	$-0.5 \times (\Delta R_{[CFB]} + 0.5 \times \Delta R_{[T2]})$	±50%

[a]Values are set in relation to a total effective greenhouse-gas radiative forcing of 3.7 W m^{-2} with an associated negative aerosol and land-surface feedback of −1.2 W m^{-2} (see **Figure 2**). In addition, the impacts of carbonate compensation and weathering are arbitrarily set in a very simple manner to each remove the forcing and immediate feedbacks related to half of the carbon emissions.
[b]The 10^5-year timescale for weathering follows the findings of Lord et al. (2016).

cloud albedo. All of these operate quasi-immediately and are here rolled into one term that also includes the impact of a single greenhouse-gas introduction within the first year ($\Delta R_{[T2]}$) because separating these impacts is not needed for the simple scenarios considered. **Table 1** summarizes the parameters and their values in this scenario.

We scale the total of the initial forcing to 3.7 W m^{-2} based on the sum of the modern effective climate forcings for CO_2, CH_4, chlorofluorocarbons, N_2O, and O_3 through 2015 (Hansen et al. 2017) (**Figure 2**). Note that this is different in nature—but confusingly similar in magnitude—to common estimates given for the radiative forcing of a doubling of CO_2 concentrations. We assign to this forcing a uniformly distributed uncertainty range of ±10% to span the reported ±0.3 W m^{-2} range of observations (**Figure 2**). We partition this 3.7 W m^{-2} (±10%) in a simple manner, into (*a*) a virtually instantaneous response of 60% ($\Delta R_{[T2]} = 2.2$ W m^{-2}) in the first year; (*b*) a somewhat slower response of (arbitrarily) 10%, resulting from snow and sea-ice albedo adjustment over a few decades ($\Delta R_{[SSI]} = 0.4$ W m^{-2}); and (*c*) a delayed temperature response of 30%, caused by surface- and deep-ocean heat uptake ($\delta_{[SO]} + \delta_{[DO]} = 1.1$ W m^{-2}) (**Table 1**). The latter is based on an observed cumulative ocean heat uptake of approximately 125×10^{21} J between 2000 and 2010 (IPCC 2013, Whitmarsh et al. 2015). We simply partition this 50:50 between the surface and deep ocean, although in reality the observed [and supported by Coupled Model Intercomparison Project 5 (CMIP5)] cumulative ocean heat uptake over the industrial era is unequally distributed, with approximately 33×10^{22} J in the upper 700 m of the ocean, 10×10^{22} J at

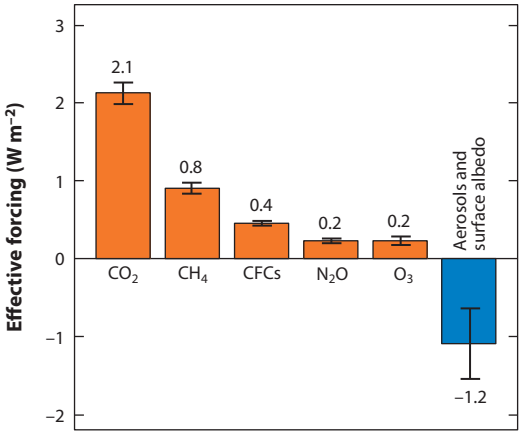

Figure 2

Estimated effective climate forcings (1750–2015) for our actuo-scenario. The forcings are based on observations of each gas except for simulated CH_4-induced changes of O_3 and stratospheric H_2O included in the CH_4 forcing. Aerosols and surface albedo change are estimated from historical scenarios of emissions and land use. Oscillatory and intermittent natural forcings (solar irradiance and volcanoes) are excluded. CFCs include not only chlorofluorocarbons, but also all Montreal Protocol trace gases and other trace gases. Uncertainty (for 5–95% confidence) is 0.6 W m^{-2} for total greenhouse-gas forcing and 0.9 W m^{-2} for aerosol forcing (Myhre et al. 2013). Data are from Hansen et al. (2005), updated to reflect the period 1750–2015 (see also Hansen et al. 2017).

700–2,000 m, and 7×10^{22} J at greater depths (Gleckler et al. 2016). The final fast feedback considered, $\Delta R_{[AE]}$, involves the albedo impacts of aerosol and land-surface changes, with timescales of up to a few decades. We scale $\Delta R_{[AE]}$ to -1.2 W m^{-2} based on the effective climate forcing of aerosols and surface albedo through 2015 (Hansen et al. 2017) and capture the reported uncertainties with a generous, uniformly distributed uncertainty range of $\pm 50\%$ (**Figure 2**, **Table 1**). Note that, by including the present-day effect of aerosols, our approach is not easily comparable with general circulation model–based results for ECS (typically obtained from $2 \times CO_2$ experiments), because aerosol impacts are not commonly included in those simulations. But aerosols are an important aspect of real-life climate change, and ignoring them would skew the results.

The fast responses $\Delta R_{[T2]}$, $\Delta R_{[SSI]}$, and $\Delta R_{[AE]}$ are followed by the influences of delayed surface-ocean (upper 2,000 m) heat uptake ($\delta_{[SO]}$) and carbon-cycle feedbacks such as permafrost and wetland releases of methane ($\Delta R_{[CFB]}$) over timescales of up to a few centuries. Even slower responses then follow, related to deep-ocean (>2,000 m) heat uptake over a millennium or two ($\delta_{[DO]}$), albedo changes caused by large-scale reorganizations of vegetation that may occur over many centuries ($\Delta R_{[VG]}$), and multicentury to millennial-scale (Grant et al. 2014) continental ice-sheet albedo adjustments ($\Delta R_{[LI]}$). The amplitudes of $\delta_{[SO]}$ and $\delta_{[DO]}$ were discussed above, $\Delta R_{[CFB]}$ is arbitrarily set to 5% of $\Delta R_{[T2]}$, and $\Delta R_{[VG]}$ is arbitrarily set to 5% of the sum $\Delta R_{[T2]} + \Delta R_{[AE]}$. Both $\Delta R_{[CFB]}$ and $\Delta R_{[VG]}$ are assigned uniformly distributed uncertainty ranges of $\pm 50\%$.

For $\Delta R_{[LI]}$, we rely on suggestions that, as long as CO_2 levels remain well below approximately 750 ppm (DeConto & Pollard 2003), ice-sheet changes affect sea levels up to approximately 20 m above the present (Foster & Rohling 2013, Rohling et al. 2013, Gasson et al. 2016). We use a median adjustment of 10 m of sea-level rise for our scenario, in agreement with peak values for the previous (Eemian) interglacial, when temperatures rose to around 1°C above present (see discussions in Hansen et al. 2013a, 2017; Hoffman et al. 2017). Reconstructions for paleo-scenarios imply that the radiative impacts of ice-sheet decay equal approximately 3 W m^{-2} per

125-m-equivalent sea-level rise (Hansen et al. 2008, Köhler et al. 2010, Rohling et al. 2012). There remains considerable uncertainty with this number; using three-dimensional ice-sheet models, Köhler et al. (2015) found it to be 4 W m^{-2}, whereas Friedrich et al. (2016) reported it to be only 1.5 W m^{-2}, likely related to a smaller simulated albedo change between land-ice-covered conditions and no-ice conditions relative to that used by Köhler et al. (2015). We use a uniformly distributed uncertainty of ±50% of $\Delta R_{[LI]}$, to allow a uniform range between 1.5 and 4.5 W m^{-2} for a 125-m-equivalent sea-level change, which spans the estimates in the literature. Hence, we set the median $\Delta R_{[LI]}$ in the actuo-scenario to $3 \times (10/125)$ W m^{-2} for a sea-level rise up to 10 m. We accept that use of this linear approximation of $\Delta R_{[LI]}$ from sea-level change obscures a potentially important nonlinearity of the climate system, which may underpin a state dependence in $S_{[CO2,LI]}$ over the last 2 million years (Köhler et al. 2015).

For each process, the above-mentioned idealized signal-development curve uses the standard functional form

$$\Delta R(t) = \frac{(h + \varepsilon_h)}{1 + e^{\left[-c\left(\frac{t}{\tau+\varepsilon_\tau} - \phi\right)\right]}}. \quad 2.$$

Here, h is the total signal amplitude (**Table 1**, with range as stated), t is time, τ is the timescale of full response (**Table 1**, with range as stated), ϕ is a translation constant (set to 0.5) to ensure that signals start at $t = 0$, and c is an acuteness constant (set to 14) to ensure that full signal amplitude is achieved over timescale τ. We run Equation 2 for each process in a Monte Carlo–style manner ($n = 1{,}000$), with random perturbations over the uniformly distributed uncertainty ranges to both h and τ (ε_h and ε_τ in **Table 1**). Note that we chose uniform distributions because the uncertainties represent not so much standard random error distributions around a mean as ranges within which parameter values may systematically shift (efficacy changes) in relation to changes in the climate background state. We then add all instances up across all processes to yield the cumulative radiative response and determine the median along with the 2.5th and 97.5th percentiles that delineate the 95% probability bounds (**Figure 3*a***; note that, for clarity of presentation, probability bounds are shown only for the cumulative total).

Next, we roughly scale the cumulative radiative response distribution, $\Delta R_{[tot]}(t)$, to a distribution of total temperature change through time, $\Delta T(t)$ (**Figure 3*b***), assuming a constant amount of temperature change per W m^{-2} of radiative change, regardless of the process. A rough scaling is sufficient because we are attempting not to model reality, but only to create a graphic illustration scenario. Our approach scales each individual Monte Carlo instance's sum of completed radiative contributions by fast forcings and feedbacks ($\Delta R_{[ff]} = \Delta R_{[T2]} + \Delta R_{[SSI]} + \Delta R_{[AE]}$) at the time point of calibration (t_{cal}, where all fast responses are completed) to a prescribed temperature change, ΔT_{tcal}. In the actuo-scenario, ΔT_{tcal} is randomly drawn from a normal distribution with a mean of 1°C and 1σ of 0.1°C, in approximation of the current amount of global warming in response to the net radiative change caused by forcing (greenhouse-gas emissions) and fast feedbacks (Hansen et al. 2013a, 2017; IPCC 2013). This yields $s_{tcal} = \Delta T_{tcal} / \Delta R_{[ff],tcal}$, which in turn gives the time series of temperature change using $\Delta T(t) = \Delta R_{[tot]}(t) \times s_{tcal}$, with propagation of all uncertainties in the various ΔR terms and in ΔT_{tcal} across all Monte Carlo instances (**Figure 3*b***).

We now have $\Delta R_{[ff]}(t)$ and $\Delta T(t)$ (**Figure 3*a*,*b***). This allows estimation of the time-dependent climate sensitivity parameter $S(t) = \Delta T(t) / \Delta R_{[ff]}(t)$ (**Figure 3*c***). Because $\Delta T(t)$ develops in response to the action of all forcings and feedbacks [$\Delta R_{[tot]}(t) = \Delta R_{[ff]}(t) + \Delta R_{[sf]}(t)$], whereas $S(t)$ depends only on $\Delta R_{[ff]}(t)$, the reconstruction of $S(t)$ continues to vary after completion of the fast processes. The conceptual equilibrium value S^a is achieved when surface-ocean warming has completed, whereas slow feedbacks have not yet become important (PALAEOSENS 2012); therefore, S^a is best identified at $t = 200$ years in our scenario. Its range reflects the propagation of all

uncertainties in all input variables, and we constrain 95% probability bounds using 2.5th and 97.5th percentiles across all 1,000 instances. **Figure 4** shows histograms for S^a.

However, there is a complication. By $t = 200$ years, the scenario's relatively rapid carbon-cycle feedbacks ($\Delta R_{[CFB]}$) have come into play. This illustrates the complexity of using a stationary

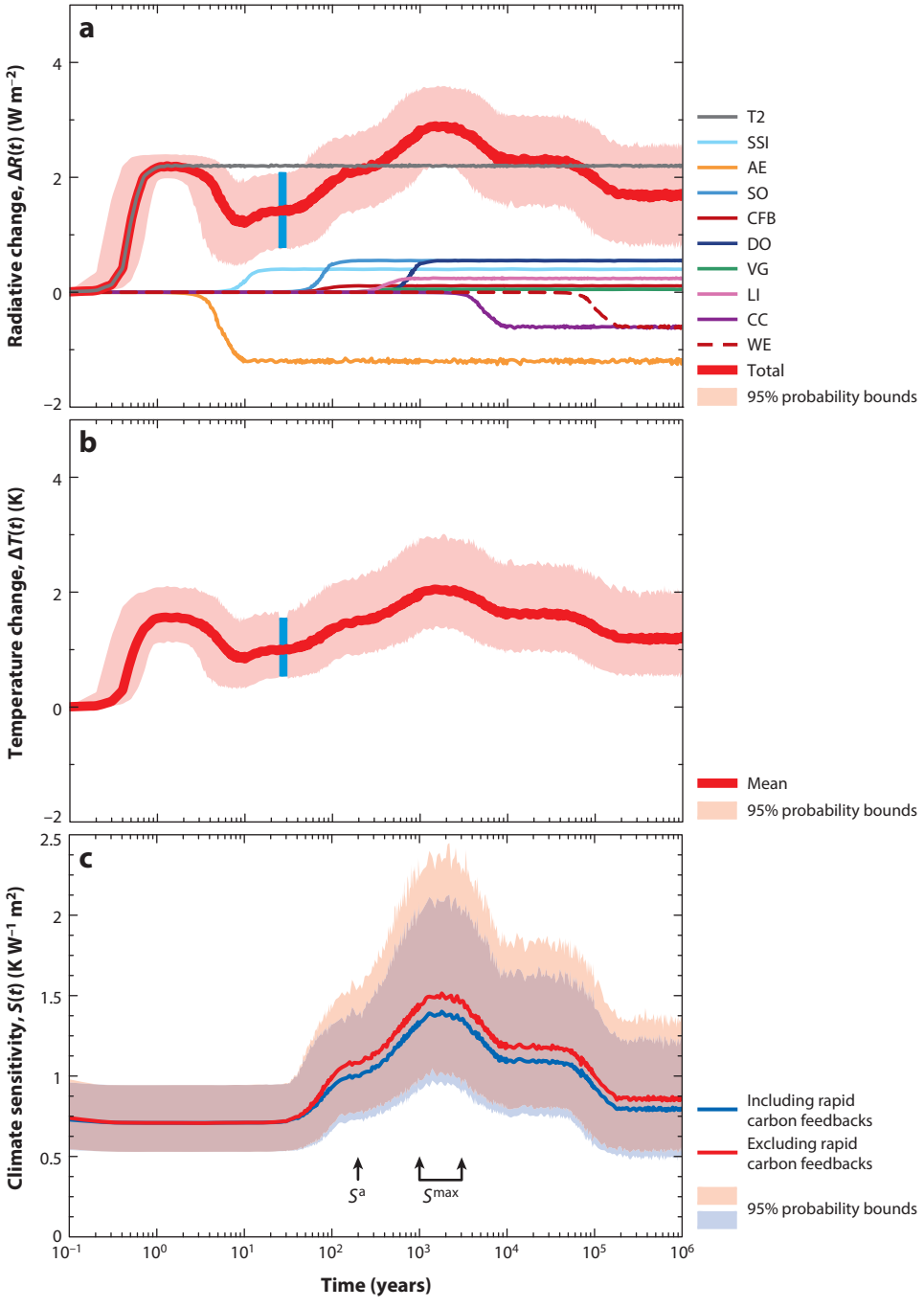

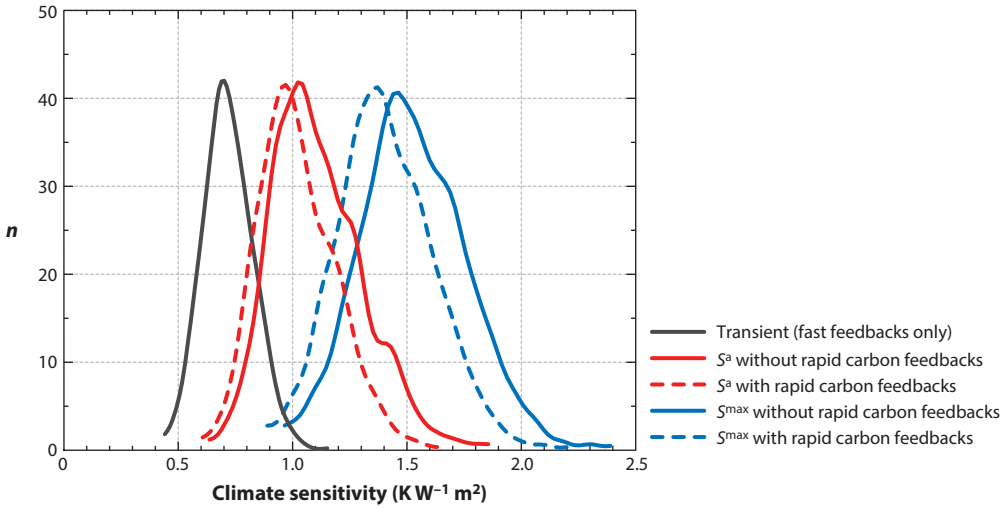

Figure 4

Histograms for our actuo-scenario. The various curves are determined at $t = 200$ years for S^{a} and as the average of $1{,}000 \leq t \leq 3{,}000$ years for S^{max}, as indicated in **Figure 3*c***.

definition to diagnose a complex, dynamic, and interconnected system. At $t = 200$, we therefore read values of S^{a} calculated with and without explicitly accounting for $\Delta R_{[CFB]}$ (see **Figure 4**). Although possible in our simple scenario, explicitly accounting for $\Delta R_{[CFB]}$ is difficult in reality because it requires knowledge of the proportion of carbon derived from feedbacks relative to that of anthropogenic external carbon input into the climate system. Hence, S^{a} without rapid carbon feedbacks (see **Figure 4**) is more relevant practically. The real climate system contains more such processes, including changes in oceanic carbon uptake efficiency in response to changes in oceanic temperature and carbon exchanges; our simple scenario illustrates the impacts of such issues but is not all-inclusive.

S^{a} at approximately $t = 200$ years still does not reflect the actuo-scenario's full development in response to the initial forcing discussed above. Even without further external forcing, the temperature continues to change (first increasing, then decreasing) because the impacts of slow processes come into play. In our scenario, the key slow processes ($\delta_{[DO]}$, $\Delta R_{[VG]}$, and $\Delta R_{[LI]}$) reach completion after approximately 1,000 years (for the land-ice-volume component in reality, this

←

Figure 3

Assessment of S^{a} in our main actuo-scenario. (*a*) Relative radiative contributions per process (showing only medians) and their total sum, along with 95% probability bounds, following the parameters outlined in **Table 1**. The number of randomly perturbed (see **Table 1**) iterations is $n = 1{,}000$. Note that $\Delta R_{[WE]}$ is a flat line at 0 W m^{-2} because it becomes important only at $t > 100{,}000$ years. The blue bar indicates the time point of calibration (t_{cal}, where all fast responses are completed). The parameters are indicated in the legend as "XX" as shorthand for "$\Delta R_{[XX]}$." (*b*) Total temperature development through time in relation to the total radiative change given in panel *c*, along with 95% probability bounds. As in panel *a*, the blue bar indicates the time point of calibration (t_{cal}, where all fast responses are completed). (*c*) Calculated $S(t)$ along with 95% probability bounds. For comparison, results are shown for two cases: one including carbon-cycle feedback ($\Delta R_{[CFB]}$) influences (*blue*) and one excluding these influences (*red*). The arrow on the left indicates where S^{a} is measured, and the two connected arrows on the right show the interval where the S^{max} estimate is taken.

may be too fast, given that adjustment over ~3,000 years has been suggested by modeling studies; Clark et al. 2016). From approximately $t = 3{,}000$ years, carbonate compensation becomes a player as the first of the very slow Earth system responses (eventually also including silicate weathering) that slowly remove the carbon. We portray the peak value of $S(t)$ (here named S^{max}) using the distribution between $t = 1{,}000$ and $t = 3{,}000$ years (see **Figure 4**). If the $\Delta R_{[LI]}$ adjustment time were stretched to ~3,000 years (see Clark et al. 2016), S^{max} would be a narrower peak of similar amplitude, centered on $t = 3{,}000$ years.

3.2. Illustrative Scenario for Paleoclimate Sensitivity

Paleoclimate sensitivity is approached differently. It relies on quantification of the slow feedbacks, notably those associated with carbon-cycle changes as expressed in greenhouse-gas records ($\Delta R_{[GHG]}$), with continental land-ice albedo changes ($\Delta R_{[LI]}$), and with vegetation albedo changes ($\Delta R_{[VG]}$). As outlined above, these slow feedbacks are effectively considered to be forcings, and their sum ($\Delta R_{[sf]}$) is used to approximate the sum of fast feedbacks ($\Delta R_{[ff]}$). The development with time in paleoclimate sensitivity is then estimated as $S_{[sf]}(t) = \Delta T(t) / \Delta R_{[sf]}(t)$. Within that time series, equilibrium paleoclimate sensitivity is identified as $S_{[sf]}$ and is reached after all slow feedbacks have reached completion. **Table 2** summarizes the parameters and their values in this scenario.

Table 2 Parameter values used in our idealized paleoclimate sensitivity scenario

Description	Code[a]	Estimated duration for full response (τ) (years)	Full range (ε_τ, uniform distribution)	Full amplitude (b) (W m^{-2})[b]	Full range (ε_b, uniform distribution)
Initial carbon-cycle (greenhouse-gas) feedbacks	$\Delta R_{[GHGi]}$	$\tau_{[GHGi]} = 50$	±50%	$\varphi \times 2.5$	±50%
Initial direct responses, including vapor and cloud feedbacks	$\Delta R_{[T2i]}$	$\tau_{[GHGi]} + 1$	±0.5 years	$\varphi \times 3$	±50%
Initial snow and sea-ice albedo feedback	$\Delta R_{[SSIi]}$	$\tau_{[GHGi]} + 20$	±10 years	$\varphi \times 2$	±50%
Initial aerosol and land-surface feedbacks	$\Delta R_{[AEi]}$	$\tau_{[GHGi]} + 10$	±5 years	$\varphi \times 1.5$	±50%
Continental ice albedo feedback	$\Delta R_{[LI]}$	$\tau_{[LI]} = 6{,}000$	±50%	3	±50%
Snow and sea-ice albedo feedback	$\Delta R_{[SSIr]}$	$\tau_{[LI]} + 20$	±10 years	$(1 - \varphi) \times 2$	±50%
Carbon-cycle (greenhouse-gas) feedbacks	$\Delta R_{[GHGr]}$	$\tau_{[SSI]} + 200$	±100 years	$(1 - \varphi) \times 2.5$	±50%
Direct responses, including vapor and cloud feedbacks	$\Delta R_{[T2r]}$	$\tau_{[GHG]} + 1$	±0.5 years	$(1 - \varphi) \times 3$	±50%
Aerosol and land-surface feedbacks	$\Delta R_{[AEr]}$	$\tau_{[LI]} + 10$	±5 years	$(1 - \varphi) \times 1.5$	±50%
Vegetation albedo	$\Delta R_{[VGr]}$	$\tau_{[LI]} + 500$	± 50 years	1	±50%

[a]Forcing amplitudes are based on a typical deglaciation within the late Pleistocene glacial cycles, as discussed by Köhler et al. (2010) and Rohling et al. (2012). Our scenario apportions values to fast-feedback contributions within a total $\Delta R_{[ff]}$ that is held proportional to the total of slow-feedback contributions, $\Delta R_{[sf]}$, following the PALAEOSENS (2012) framework. The radiative subdivisions for the various fast feedbacks are irrelevant and used here only for illustration. For $\Delta R_{[GHG]}$, $\Delta R_{[T2]}$, $\Delta R_{[SSI]}$, and $\Delta R_{[AE]}$, we incorporate a schematic representation of an initial rapid response to the onset of deglaciation (indicated in the code with "i") and a second, remaining component (indicated in the code with "r") that is delayed as it coevolves with ice-volume reduction.

[b]The proportion of the initial responses is set by factor φ, which we tentatively set at 0.15; initial responses are set to start with initial carbon-cycle responses within 25–75 years after the initial (orbital insolation) perturbation. Changing these values does not materially affect our conclusions.

Conceptually, no immediate agreement might be expected between actuo- and paleoclimate sensitivity estimates because they are determined from processes operating over very different timescales, with different assumptions and uncertainties. For example, past climate variations were not adjustments to very rapid, high-amplitude perturbations (such as the anthropogenic CO_2 emissions) along the lines of actuo-climate adjustments, but were triggered by slowly developing processes such as orbital forcing, with timescales of many thousands of years. Hence, paleoclimate records reflect coevolving changes in all climate-regulating processes (save for the very slowest ones, such as plate tectonics) that are either in or near equilibrium with the changing forcing. As a consequence, most studies based on time series of temperature and slow-feedback change directly find the equilibrium value $S_{[sf]}$, although this may not be true in highly resolved studies over centennial-to-millennial-scale climate fluctuations (see below). In addition, paleoclimate records represent an integration of all feedback processes; e.g., they include not only the temperature response to CO_2 changes, but also the CO_2 response to temperature changes. Our simple paleo-scenario allows such complications to be teased apart, to gauge over what timescales signals need to be considered to approximate the desired equilibrium sensitivity and what the consequences would be of pushing reconstructions from paleodata into shorter timescales.

For the scale and duration of the processes in our paleo-scenario, we draw on studies of glacial cycles of the last 800,000 years. As such, this scenario may be seen as a rough approximation of a deglaciation. Deglaciations were triggered by orbital forcing of climate, in particular by changes in Northern Hemisphere summer insolation (Hays et al. 1976). Orbital forcing involves minor annual-mean global-mean forcing ($\ll 0.5$ W m^{-2}) but sets up considerable gradients on spatial (latitudinal) and seasonal scales. For a long time, it was not well understood how these triggered deglaciations (Shackleton 2000, Denton et al. 2010, Abe-Ouchi et al. 2013), although the timing relationship was reasonably clear (Hays et al. 1976, Cheng et al. 2016). Recently, a simple model has related every deglaciation of the last million years to the crossing of summer insolation through a simple threshold (Tzedakis et al. 2017).

Our paleo-scenario considers an idealized sequence of events inspired by data for the penultimate glacial termination (Marino et al. 2015, Holloway et al. 2016) because this termination avoids the greater complexity of the last deglaciation yet still has the requisite chronological control for the relevant climate records (Billups 2015, Marino et al. 2015). Following the initial perturbation (orbital forcing) and fast responses, continental ice-volume changes over thousands of years drove the further feedback responses mainly through bipolar temperature seesaw processes (Stocker 1998, Stocker & Johnsen 2003) that led to rapid Southern Ocean warming and sea-ice reduction, CO_2 outgassing, warming and vapor feedbacks, and so on. Here we include aerosol changes in that suite as well, despite a lack (so far) of unequivocal empirical evidence of that particular coupling. There is no unambiguous empirical evidence about the phase relationship of global mean vegetation responses to ice-volume changes, either. But given that we seek only to formulate an illustrative, idealized scenario, we simply assume that key vegetation changes take place within centuries following land-ice changes.

The orbital-forcing component is ignored here because of our focus on annual-mean global-mean forcing. But it is important in that it directly triggers responses in ice sheets and other processes in the climate system (Schmidt et al. 2017), which cause additional feedback responses once the climate begins to change; some of these links develop rapidly, and others develop slowly. For example, small, regionally or seasonally focused warming resulting from orbital forcing triggers sea-ice retreat as well as changes in surface albedo and air-sea carbon exchange, which drive further warming, and so on. Thereafter, the slow feedbacks come into action, such as land-ice and vegetation albedo changes. When that happens, fast processes keep interacting with slow feedbacks. Paleo-reconstructions cannot distinguish fast responses associated with slow processes

from the slow processes themselves, or indeed the acceleration of slow processes resulting from associated, superimposed fast responses. Note that similar interactions occur in actuo-climate changes, but our simple actuo-scenario avoids this issue by pragmatically viewing the stipulated slow-feedback influences as effective net impacts. Doing so in the paleo-scenario would divorce our scenario too much from the paleo-reconstructions, in which temperature (and fast feedbacks) closely coevolve over thousands of years with the slow feedbacks (e.g., Rohling et al. 2009; Grant et al. 2012, 2014). Because our simple paleo-scenario cannot resolve such interactions (a dynamic model would be needed), we instead include a crude representation by evaluating the contribution of fast feedbacks to paleoclimate change as a two-stage development. One stage stands for the initial responses (indicated in **Table 2** with "i" in the parameter names), and the other is the subsequent fast-feedback response (indicated with "r") associated with the development of the dominant slow continental land-ice feedback ($\Delta R_{[LI]}$). We tentatively set 0.15:0.85 proportionalities for this. The proportionality is crudely inspired by early (initial) CO_2 jumps that predate significant ice-volume/sea-ice responses, at around 16,300, 14,800, and 11,700 years ago, with CO_2 levels in each case jumping abruptly by approximately 15% of the total deglacial change (Lambeck et al. 2014, Marcott et al. 2014).

To obtain $S_{[sf]}$, slow feedbacks are effectively considered to be climate forcings in the PALAEOSENS (2012) framework. Our scenario considers the total greenhouse-gas forcing component $\Delta R_{[GHG]}$. In paleodata studies, this component can be determined from records of greenhouse-gas changes (notably from ice cores). These records integrate all carbon-cycle feedbacks, including carbonate compensation and weathering, which therefore need not be considered separately. We then add the continental land-ice albedo effect, which can be found from sea-level reconstructions, giving $\Delta R_{[GHG]} + \Delta R_{[LI]}$. Finally, the slow vegetation albedo feedback ($\Delta R_{[VG]}$) should be similarly accounted for, but this is substantially challenged by an absence of good global data coverage, which definitely needs to be addressed through future research. To date, hardly any paleo-studies have accounted for $\Delta R_{[VG]}$ (Friedrich et al. 2016 is an exception), and we assess the implications by showing results that either include or exclude $\Delta R_{[VG]}$. Our analysis does not include albedo changes caused by atmospheric dust (aerosol) variations among the slow feedbacks/forcings, because there is no agreed way to deal with aerosols in paleoclimate sensitivity studies and because time series of atmospheric dust are geographically very limited and generally qualitative anyway, so that the aerosol component remains highly speculative and uncertain (e.g., PALAEOSENS 2012, Rohling et al. 2012).

We roughly calibrate or scale our paleo-scenario on the basis of values for the radiative forcings and feedbacks compiled by Köhler et al. (2010) and Rohling et al. (2012) (**Table 2**), with a total median value of 3 W m^{-2} for $\Delta R_{[LI]}$ (for discussion, see Section 3.1) and 2.5 W m^{-2} for $\Delta R_{[GHG]}$. We use $\Delta R_{[VG]} = 1$ W m^{-2}, in agreement with Friedrich et al. (2016). As in the PALAEOSENS (2012) framework, we assume that $\Delta R_{[ff]}$ is proportional to $\Delta R_{[sf]}$ over timescales of more than a few thousand years. On shorter timescales, this assumption cannot be correct because fast feedbacks dominate at first, whereas slow feedbacks become important at a later stage (our results illustrate this). Proportional contributions of individual fast responses are irrelevant here because our assessment always considers their summed value, but just for illustration's sake, we have made an attempt at reasonably apportioning them (**Table 2**). The total median range of $\Delta R_{[AE]}$ is estimated at around 1.5 W m^{-2}, and for snow and sea-ice albedo we use $\Delta R_{[SSI]} = 2$ W m^{-2}, based on discussions by Köhler et al. (2010) and Rohling et al. (2012). This leaves 3 W m^{-2} for the outgoing long-wave radiation response, water-vapor content, atmospheric lapse rate, cloud albedo, and so on, all of which are captured in one term, $\Delta R_{[T2]}$. All radiative terms are assigned ±50% uncertainties using uniform distributions. The paleo-scenario omits $\delta_{[SO]}$ and $\delta_{[DO]}$ because paleodata yield only the total temperature response, which includes these factors.

The median and 95% uncertainty limits (2.5th and 97.5th percentiles) are determined from our Monte Carlo statistics ($n = 1{,}000$) for the sum of all completed forcings and feedbacks ($\Delta R_{[tot]} = \Delta R_{[ff]} + \Delta R_{[sf]}$) (**Figure 5*a***). From this, we determine $\Delta T(t)$ (**Figure 5*b***), assuming a constant amount of temperature change per W m^{-2} of radiative change. To do so, we scale each Monte Carlo instance's sum of all completed radiative contributions ($\Delta R_{[tot]}$), taken at $t_{cal} = 10{,}000$ years (see **Figure 5*a***), to a temperature change ΔT_{tcal}. The latter is randomly drawn from a normal distribution set to a mean of 5°C and 1σ of 1°C. This gives $s_{tcal} = \Delta T_{tcal} / \Delta R_{[tot],tcal}$, and thus the temperature time series $\Delta T(t) = \Delta R_{[tot]}(t) \times s_{tcal}$, with propagation of all uncertainties in the various ΔR terms and in ΔT_{tcal} across all Monte Carlo instances (**Figure 5*b***). The final range of temperature uncertainties (**Figure 5*b***) spans the entire range of proposed, and still debated, glacial-interglacial temperature-change estimates of Hansen et al. (2007), MARGO (2009), Köhler et al. (2010), Masson-Delmotte et al. (2010), Schmittner et al. (2011), Rohling et al. (2012), Annan & Hargreaves (2013), and Snyder (2016).

Based on the time series $\Delta R_{[ff]}(t)$, $\Delta R_{[sf]}(t)$, and $\Delta T(t)$, we calculate $S_{[sf]}(t) = \Delta T(t) / \Delta R_{[sf]}(t)$ as in the PALAEOSENS (2012) framework, as well as $S_{[ff]}(t) = \Delta T(t) / \Delta R_{[ff]}(t)$, which is more directly comparable to S^a from the actuo-scenario (**Figure 5*c***). Comparison between $S_{[sf]}(t)$ and $S_{[ff]}(t)$ highlights the controls on their similarities and differences. Note that calculating $S_{[ff]}(t)$ is possible in this simple scenario but not in real paleodata studies. There is also a complication in that part of $\Delta R_{[sf]}$ consists of $\Delta R_{[VG]}$, which is still poorly understood in real paleodata studies. Hence, most such studies use a pragmatic approximation of $\Delta R_{[sf]}$, which is just $\Delta R_{[GHG]} + \Delta R_{[LI]}$. Here we determine both versions, one with and one without $\Delta R_{[VG]}$, to illustrate how this limitation affects the results.

The results for $S_{[sf]}(t)$ and $S_{[ff]}(t)$ only begin to fully converge at around $t = 5{,}000$ years (**Figure 5*c***) because of a predominance of the fast feedbacks on short timescales and an increased relative importance of slow feedbacks on longer timescales. We read estimates for the equilibrium paleoclimate sensitivity parameter $S_{[sf]}$ as the average of values between $t = 8{,}000$ and $t = 10{,}000$ years. **Figure 6** shows histograms for our paleo-scenario. The exact convergence between $S_{[sf]}(t)$ and $S_{[ff]}(t)$ in the scenario with $\Delta R_{[sf]} = \Delta R_{[GHG]} + \Delta R_{[LI]} + \Delta R_{[VG]}$ results from the PALAEOSENS (2012) argument that $\Delta R_{[ff]}$ approximates $\Delta R_{[sf]}$. However, **Figures 5*c*** and **6** show that the common pragmatic limitation of $\Delta R_{[sf]} = \Delta R_{[GHG]} + \Delta R_{[LI]}$ (without $\Delta R_{[VG]}$) overestimates long-term values for $S_{[sf]}(t)$ by almost 20%.

4. DISCUSSION

4.1. Comparison Between S^a and $S_{[sf]}$

It stands out strongly from **Figure 3** for the actuo-scenario that any reported S^a value needs to be carefully referenced to the processes that are included. This is commonly done using a rather arbitrary timescale of 100 years, which is then considered to give the ECS that includes all fast processes and surface-ocean warming but excludes slow processes (PALAEOSENS 2012). It is interesting, however, to compare this approach with models, where one can check when equilibrium is reached. For example, Hansen et al. (2011) showed that, in the Goddard Institute for Space Studies ModelE-R, surface-ocean equilibration to instantaneous forcing is just 60% complete after 100 years, reaching ~100% only after as much as 2,000 years (their figure 3). In addition, in runs longer than 100 years in most models, the relationship between energy imbalance and temperature change that is used to extrapolate ECS (the so-called Gregory method; Gregory et al. 2004) breaks down from an assumed linear relationship to a nonlinear one (Bloch-Johnson et al. 2015, Rugenstein et al. 2016b, Proistosescu & Huybers 2017). In addition, as mentioned

Figure 5

Assessment of $S_{[sf]}$ in our main paleo-scenario. (*a*) Relative radiative contributions per process (showing only medians) and their total sum, along with 95% probability bounds, following the parameters outlined in **Table 2**. The number of randomly perturbed (see **Table 2**) iterations is $n = 1{,}000$. The blue bar indicates the time point of calibration (t_{cal}, in this case where the full response has been completed). The parameters are indicated in the legend as "XX" as shorthand for "$\Delta R_{[XX]}$." (*b*) Total temperature development through time, in relation to the total radiative change given in panel *c*, along with 95% probability bounds. As in panel *a*, the blue bar indicates the time point of calibration (t_{cal}, where the full response has been completed). (*c*) Calculated paleoclimate sensitivity along with 95% probability bounds for different definitions. The two connected arrows on the right show the interval where the $S_{[sf]}$ estimate is taken.

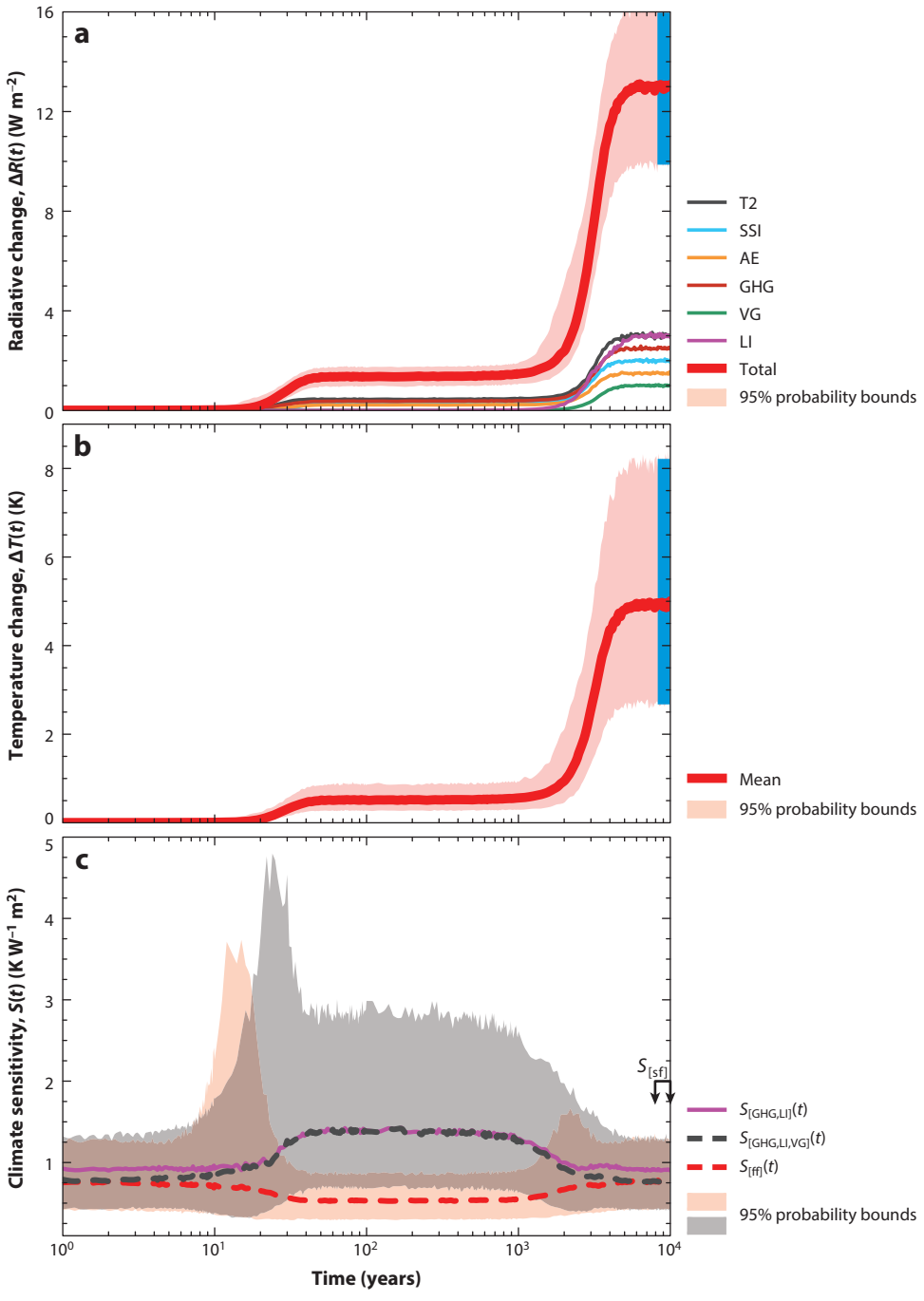

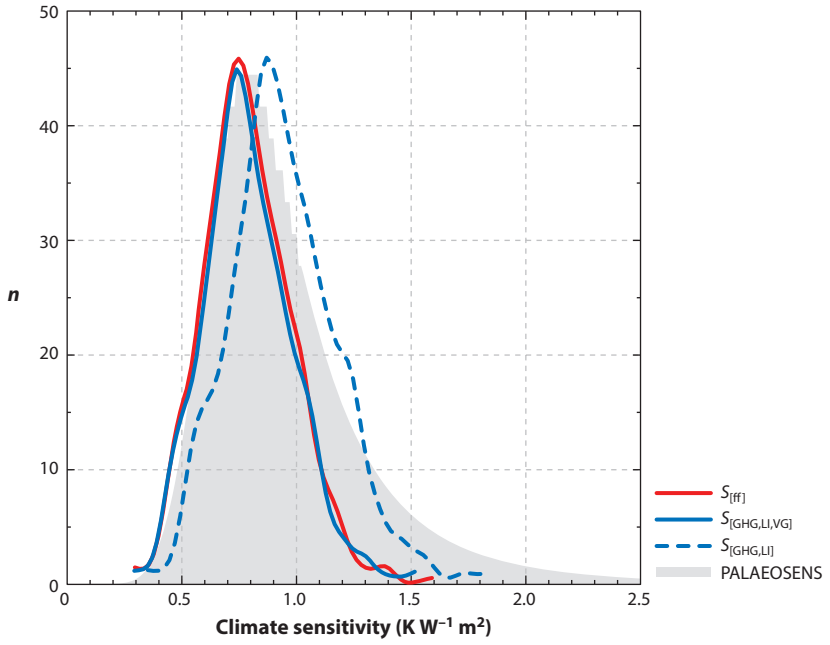

Figure 6

Histograms for our paleo-scenario. The various curves are determined as the averages of $8{,}000 \leq t \leq 10{,}000$ years, as indicated in **Figure 5*c***. The gray shading represents a scaled version of the distribution from PALAEOSENS (2012, their figure 3*c*).

above, any comparison of our number for S^a with general circulation model–based ECS estimates is complicated by the fact that model simulations typically start with a perturbation of CO_2 but omit the observed negative radiative impacts from anthropogenic aerosols and land-surface changes (**Figure 2**), which act to reduce the temperature rise.

Clearly, even our simple scenario does not neatly separate processes in time. Uncertainties in the timescales of the various processes and the potential operation of $\Delta R_{[CFB]}$ on similar timescales to $\delta_{[SO]}$ make climate sensitivity a moving target through time (**Figure 3**). For the example set up here, $t = 200$ years seems more suitable for determining S^a because all included responses (fast feedbacks) have completed (although this is not fully the case in the more realistic model of Hansen et al. 2011). However, even in our simple scenario, $t = 200$ years does not provide a clear-cut criterion because the estimate then includes $\Delta R_{[CFB]}$, which should in that case be corrected for to match the definition of ECS (**Figures 3*c*** and **4**). And in reality, there will be further carbon-cycle processes causing similar issues, as discussed in Section 3.1. Therefore, although exact definitions of included processes and better determination of the timescales of the different contributing response functions are needed to obtain S^a estimates that are as precise as possible (and as comparable between studies as possible), it is not obvious that such a level of distinction will always be possible in a natural system.

Figure 3*c* also shows that, if an arbitrarily selected cutoff time for S^a assessment causes partial inclusion of ongoing slow processes (e.g., surface-ocean warming), then this may cause extended tails to the probability distribution function (PDF) of the climate sensitivity estimate. In particular, if this PDF were made by collating information from different climate models, each with different representations of the myriad processes and their timescales, then the combined PDF may

become very broad. A narrower combined PDF might be obtained by identifying the contributions of each process to climate sensitivity in each model and then comparing results not at a certain time step, but instead at a certain well-defined point that is based on exactly which processes are included and which are not. This point may occur at different time steps in different models. This approach would be a more process-oriented way of comparing between models than a simple comparison between their results at an arbitrarily selected moment in time, where different processes contribute to different degrees in different models. Also note that our use of uniform distributions for the various parameter uncertainties limits the potential skew and the potential for long tails in the calculated final PDFs (**Figure 3**) relative to results based on ratios between Gaussian-shaped PDFs for ΔT and ΔR (Köhler et al. 2010). We consider our approach justified by the fact that most uncertainties concern not random error around mean estimates but ranges of potential systematic (e.g., state-dependent) shifts of the means for many feedback efficacies. In reality, the uncertainty ranges may be more complicated, combining both systematic and random components.

Now we get to the critical question about which process-based definitions would be needed for the best comparison of S^a from actuo-studies with $S_{[sf]}$ in paleo-studies. One issue concerns the above-mentioned impacts of relatively fast carbon-cycle feedbacks ($\Delta R_{[CFB]}$ and similar additional ones in reality; see Section 3.1) on how S^a is estimated in actuo-studies. In addition, **Figures 5*c*** and **6** illustrate how a lack of explicit accounting for $\Delta R_{[VG]}$ in the most commonly used specific paleoclimate sensitivity term ($S_{[GHG,LI]}$) risks a considerable overestimate of the inferred climate sensitivity value (almost 20% in our simple scenario), making it an inaccurate approximation of $S_{[ff]}$ and therefore S^a. This clearly illustrates why resolving vegetation albedo impacts on the radiative balance of climate needs priority in data-based reconstructions of paleoclimate sensitivity.

Next, **Figure 5*c*** suggests that—regardless of the definition used—pushing paleoclimate sensitivity reconstructions from time series of paleodata to temporal resolutions of less than 5,000 years may result in overestimates of paleoclimate sensitivity because of transient behavior in the solution. This suggests that paleoclimate sensitivity reconstructions through, for example, North Atlantic Heinrich events or the Younger Dryas may yield unstable results, with potential anomalies to high values. Yet it may be instructive to carefully reconstruct time series of paleoclimate sensitivity in high temporal resolutions to see whether such transient anomalies are actually found and, if so, when and how they settle toward equilibrium values. Accurate reconstruction of global mean temperature changes will be vital to such assessments because a large component of the temperature swings through such events may concern energy redistribution around the globe (Stocker 1998) rather than global mean change. Establishing the transient behavior of paleoclimate sensitivity might uncover interesting clues about the critical real-world processes involved and their timescales.

Finally, paleoclimate studies can measure only the full temperature response, which includes the delayed ocean responses $\delta_{[SO]}$ and (part or all of) $\delta_{[DO]}$. For a sound like-with-like comparison, a truly equilibrated actuo-scenario should therefore include these responses as well. As shown above, inclusion of $\delta_{[SO]}$ brings a conflict with potential contributions of $\Delta R_{[CFB]}$ in the actuo-scenario (**Figure 3**). In time-series-based paleoclimate studies, individual carbon-cycle components cannot be distinguished, so the best comparison between S^a from actuo-studies and paleo-$S_{[sf]}$ estimates would require exclusion of any $\Delta R_{[CFB]}$ influences (and/or similar carbon-cycle changes; see Section 3.1) from the S^a estimate. The situation is worse with respect to the slow $\delta_{[DO]}$. Including this in an S^a estimate from actuo-studies would require consideration over thousands of years, by which time carbonate compensation, continental land-ice influences, and long-term vegetation adjustments would also have become important players in the temperature developments (**Figure 3**). In addition, inclusion of $\delta_{[DO]}$ would increase the timescale of evaluation to a few

thousand years rather than a century or two into the future, which reduces the apparent relevance to society. For pragmatic reasons, S^{a} is defined to include $\Delta R_{[T2]}$, $\Delta R_{[SSI]}$, $\Delta R_{[AE]}$, and $\delta_{[SO]}$, and it is inevitable that this imposes some limitations on precise comparability with paleoclimate-based $S_{[sf]}$ estimates.

4.2. The Dependence of Paleoclimate Sensitivity on Feedback Efficacy Changes

Efficacies of the various processes (in essence, their contributing amplitudes) are reasonably understood for the present day, where there are many observations to constrain the inferred ranges of variation. But as we transition into a much warmer world, the potential for efficacy changes in key feedbacks cannot be excluded and must be considered. For example, the efficacy of the snow and ice albedos may change as latitudinal distributions of snow and ice change, affecting the amount of (latitude-dependent) insolation reflection per unit area, and the efficacies of the fast water-vapor and cloud feedbacks may also change with background temperature (e.g., Caballero & Huber 2013; von der Heydt et al. 2014, 2016; Köhler et al. 2015). The uncertainty ranges allowed in the actuo-scenario yield wide tails in the climate sensitivity distributions, especially at the high end (**Figures 3** and **4**). A possible approach to constrain the width of the tails would be to perform large ensembles of runs over wide parameter spaces with a more representative climate model over the historical period, excluding runs that do not agree with historical time series of climate data and then determining climate sensitivity from the remaining runs.

As it is, our simple actuo-scenario's estimates for S^{a} are reached after approximately 200 years and range over a 95% probability envelope of 0.8–1.6 K W^{-1} m^2 around a median of 1.1 K W^{-1} m^2 for the case that does not explicitly account for $\Delta R_{[CFB]}$, and 0.7–1.4 K W^{-1} m^2 around a median of 1.0 K W^{-1} m^2 for the case that does explicitly account for $\Delta R_{[CFB]}$. The equilibrium value therefore is approximately 1.5 times the scenario's transient climate sensitivity value before $\delta_{[SO]}$ involvement, which has a 95% range of 0.5–0.9 K W^{-1} m^2 around a median of 0.7 K W^{-1} m^2 (see **Figure 3*a*,*c***).

Our actuo-scenario's peak values, which mark the time when slow feedbacks have also made their maximum contribution (S^{max}), have a 95% probability range of 1.0–2.3 K W^{-1} m^2 around a median of 1.5 K W^{-1} m^2 for the case that does not explicitly account for $\Delta R_{[CFB]}$, and 1.0–2.1 K W^{-1} m^2 around a median of 1.4 K W^{-1} m^2 for the case that does explicitly account for $\Delta R_{[CFB]}$. These values are achieved after approximately 1,000 years and indicate a level of approximately twice the scenario's transient climate sensitivity value.

The efficacies in the paleo-scenario are notably less constrained and may depend considerably on the climate background state (Köhler et al. 2015, Friedrich et al. 2016, von der Heydt et al. 2016). Our scenarios, using either $S_{[GHG,LI,VG]}$ or $S_{[GHG,LI]}$, include the cumulative impacts of efficacy variations in all feedbacks over ±50% ranges (uniformly distributed) (**Figures 5*c*** and **6**). For $S_{[GHG,LI,VG]}$, we find an equilibrium 95% probability range of 0.4–1.3 K W^{-1} m^2 around a median of 0.8 K W^{-1} m^2. For the more common approximation in paleo-studies, $S_{[GHG,LI]}$, we find an equilibrium 95% probability range of 0.5–1.6 K W^{-1} m^2 around a median of 0.9 K W^{-1} m^2 (**Figures 5*c*** and **6**). The latter estimate is the most useful one for comparison with published equilibrium paleoclimate sensitivity estimates because those typically were not corrected for $\Delta R_{[VG]}$ either.

With total 95% bounds of 0.4–1.6 K W^{-1} m^2, our assessments for $S_{[GHG,LI]}$ and $S_{[GHG,LI,VG]}$ closely approximate the 95% bounds of 0.3–1.9 K W^{-1} m^2 for similarly defined, observation-based estimates for the last 65 million years (PALAEOSENS 2012) (**Figure 6**). We infer, in agreement with Köhler et al. (2015), that the wide range in the PALAEOSENS (2012) framework likely results from integration of observations across a range of state-dependent paleoclimate sensitivity

values through time. This is an important point: It would seem that the width of previously reconstructed paleoclimate sensitivity distributions is not so much a function of random (proxy-based) measurement uncertainties, but instead is driven primarily by the integration of numerous, hitherto unrecognized, narrower state-dependent distributions. Given that the width of our simple scenario's range agrees well with that found from observations, we tentatively infer that overall efficacy changes through time likely remained within roughly ±50%. A caveat here is that our scenarios do not include cloud feedback mechanisms (Ceppi et al. 2017), either directly or through interaction with ocean heat uptake (Rose & Rayborn 2016), which are commonly held to be a key contributor to uncertainties in (the broad range of) climate sensitivity estimates. Such processes may significantly affect both actuo- and paleoclimate sensitivity reconstructions, but certainly for paleo-cases cannot be resolved because no method exists to reconstruct past cloud cover and types, and we are not aware of any long-term simulations with models that include realistic cloud (micro)physics.

Finally, we compare results between **Figures 4** and **6**. At 0.7–1.6 K W^{-1} m^2 around a median of 1.0–1.1 K W^{-1} m^2, S^a from our actuo-scenario appears to be slightly higher than $S_{[sf]}$ from the paleo-scenario, at 0.4–1.6 K W^{-1} m^2 around a median of 0.8–0.9 K W^{-1} m^2. However, this slight offset likely results from differences in the way the calculations have been constrained between the scenarios. With respect to the distribution width difference, we see potential for paleo-studies to provide $S_{[sf]}$ distributions that portray real total climate-system responses that represent real-world realizations of climate change, and for careful work (especially with respect to chronological relationships between time-series of data) to eventually deconvolve the overall probability distributions into narrower ones that account for climate-state dependence. Thus, paleodata studies may provide key templates (prior distributions) for exercises to select best-matching subsets from model mega-ensemble assessments of future climate developments.

Finally, we consider the question of how to tease out state dependence from paleodata using carefully designed experiments (**Figure 5**). It cannot be excluded that this will be possible, but the apparent size of the 95% probability envelope for individual scenarios suggests that estimates for different climate states are likely to overlap, except in extremely contrasting cases.

4.3. Comparison with Other Approaches

Although the above conceptual framework is different in its focus on the time domain, it follows the general principles laid out by PALAEOSENS (2012) and further explored by Royer (2016). Yet the framework's focus on radiative forcing anomalies to calculate temperature change and climate sensitivity may be less familiar to climate modelers. Therefore, we here assess the implications of a focus on the time domain in a framework of feedback analysis.

Classically, a perturbation of the radiative forcing ΔR_F—for example, by an instantaneous doubling of atmospheric CO_2 concentrations—leads to a temperature anomaly $\Delta T(t) = -\Delta R_F / \Sigma \lambda_i(t)$, where the sum of feedback parameters consists of the Planck feedback ($\lambda_P = -3.2$ W m^{-2} K^{-1}) responsible for a rise in the outgoing long-wave radiation, the sum of all other fast feedbacks ($\lambda_{other\text{-}ff}$ for surface albedo, water vapor, lapse rate, and clouds), and contributions from ocean heat uptake efficiency (κ) to the surface and deep ocean (e.g., Rose & Rayborn 2016, Rugenstein et al. 2016a). The latter are in the classical framework not called feedbacks (Dufresne & Bony 2008) but can still be calculated as such. In our example demonstration of how this framework works (**Figure 7**), these feedbacks are parameterized based on multimodel results from CMIP3 (Dufresne & Bony 2008). Although newer (CMIP5) results have been published (Vial et al. 2013), these results include a forcing adjustment, which we prefer to ignore here because it complicates the system and might be negligible in the paleo-framework.

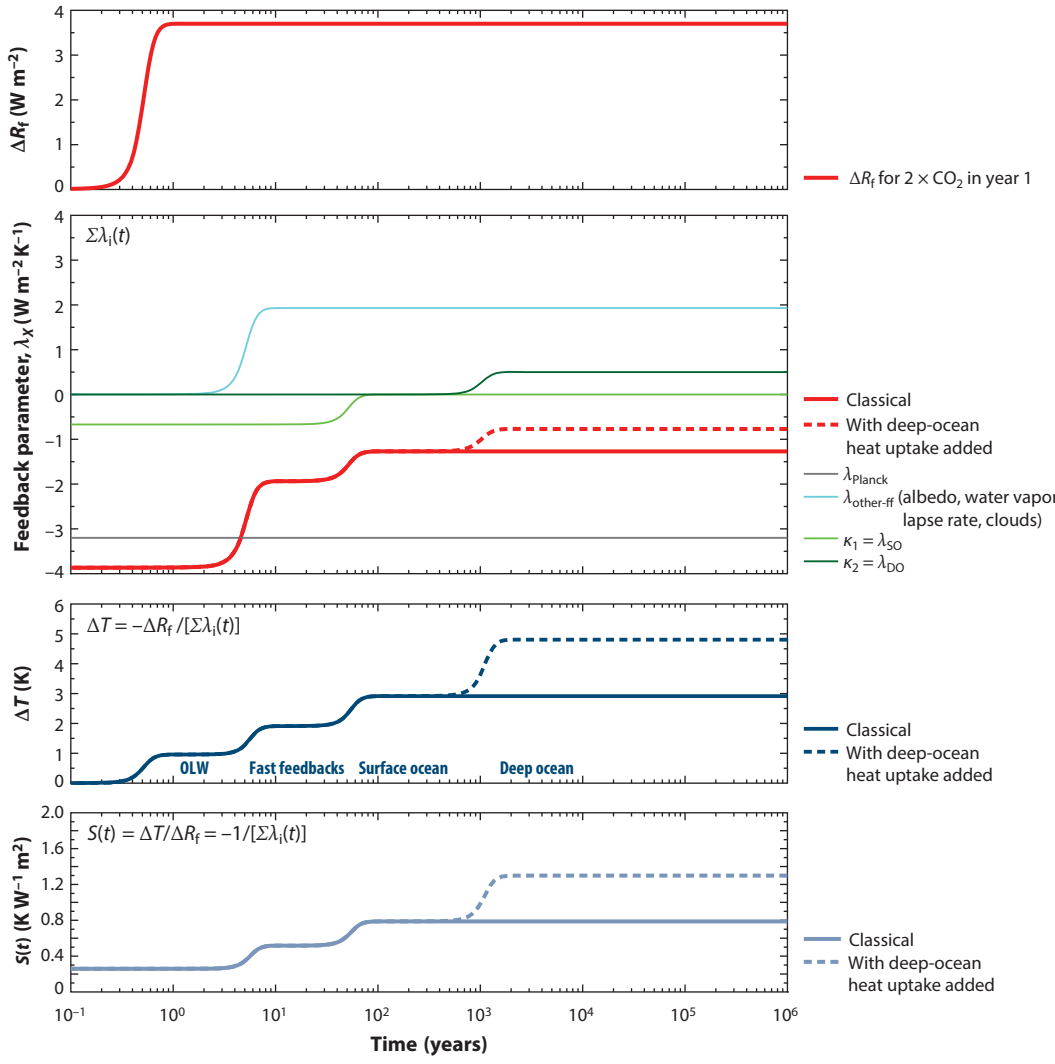

Figure 7

Analysis of the classical 2 × CO_2 experiment in a feedback analysis framework. An initial perturbation in the radiative forcing, ΔR_F, leads without any further feedbacks to the Planck response [change in outgoing long-wave radiation (OLW)], which is enhanced by further time-dependent feedback terms, $\lambda_i(t)$.

We thus end up with a time-dependent term for $\lambda_{other\text{-}ff} = +1.9$ W m^{-2} K^{-1}, which is modulated with signal development similar to that given in Equation 2 to obtain the full amplitude with $\tau = 10$ years. The pure Planck feedback then leads to a temperature rise of approximately 1 K after the first year and, together with the fast feedbacks, to approximately 2 K after a decade, in agreement with recent estimates of the transient climate sensitivity (Storelvmo et al. 2016). Adding the ocean heat uptake efficiency to the surface ocean (κ_1 or $\lambda_{SO} = -0.67$ W m^{-2} K^{-1}, with $\tau = 100$ years) then leads to a temperature rise of 3 K after a century and to a rise in the time-dependent specific climate sensitivity $S(t) = \Delta T/\Delta R_F$ from 0.52 K W^{-1} m^2 after a decade to 0.79 K W^{-1} m^2 after a century, in agreement with the estimate of ECS in CMIP3. Taking

into account that model simulations underlying the classical calculations of ECS are not in full equilibrium (Gregory et al. 2004, Hansen et al. 2011, Bloch-Johnson et al. 2015, Rugenstein et al. 2016b), one might define deep-ocean heat uptake efficiency as another feedback parameter (κ_2 or $\lambda_{DO} = 0.5$ W m^{-2} K^{-1}, with $\tau = 2{,}000$ years) that leads to a further temperature rise to a ΔT of up to 5 K on a multimillennial timescale.

Similar to this $2 \times CO_2$ example, one might translate the radiative forcing anomalies for our actuo- and paleo-scenarios (as summarized in **Tables 1** and **2**) into a framework of feedback analysis. This would yield figures similar to **Figure 7** but no new insights with respect to the time dependence of *S*, and therefore we do not evaluate it further here.

5. SUMMARY AND FUTURE ISSUES

We have analyzed and compared approaches for determining climate sensitivity in studies of modern/future (actuo) and past (paleo) climate, using graphical illustrations based on highly idealized scenarios. This reveals problems with determining a unique value for ECS in both actuo- and paleo-scenarios, because the processes involved are not strictly separated in time and/or are insufficiently understood for a sound quantification. In addition, there are issues with understanding the efficacies of the dominant processes (particularly for the paleo-scenario), which likely underpin the state dependence of climate sensitivity and the length of the tails of reconstructed climate sensitivity PDFs. The analysis presented here suggests that the width of previously reconstructed paleoclimate sensitivity distributions likely reflects the integration of numerous state-dependent distributions.

There are several key requirements for advancing the debate: (*a*) Precise chronological control is needed when comparing different proxy records of global temperature changes and forcings or feedbacks; (*b*) new approaches or strategies for reconstructing mean global temperature changes from paleo-studies are needed, given that even reconstructions through the Last Glacial Maximum disagree over a wide range; and (*c*) model-independent ways of evaluating the records are needed to avoid introducing model-dependent artifacts in the calculated climate sensitivities (i.e., circular reasoning). Furthermore, there is a continued need for (*a*) a refined understanding of how certain parameters (e.g., mean global temperature or CO_2 concentrations) are estimated with different proxies (method intercomparison studies), (*b*) detailed descriptions of assumptions and uncertainties and transparent and complete propagation of these into the calculated sensitivity distributions, (*c*) careful and transparent definition of which terms exactly are being compared between case studies, and (*d*) elaboration of high-quality records for the major missing slow feedback (vegetation).

Finally, we infer that the main focus in current work concerns the potential climate-background-state dependence of climate sensitivity. Our analysis suggests that it will be challenging to statistically robustly confirm this using paleodata. No doubt this problem will continue to receive a significant amount of attention within the next few years, and hopefully innovative approaches will be developed to constrain this critical aspect. In our view, a better understanding of feedback efficacy changes through time will be critical to sufficiently reducing uncertainties for the statistical distinction of state dependence in climate sensitivity.

DISCLOSURE STATEMENT

The authors are not aware of any affiliations, memberships, funding, or financial holdings that might be perceived as affecting the objectivity of this review.

ACKNOWLEDGMENTS

E.J.R. and G.M. acknowledge support from the Australian Research Council via Australian Laureate Fellowship FL120100050. A.S.v.d.H. acknowledges support from the Netherlands Earth System Science Centre, financially supported by the Ministry of Education, Culture, and Science. P.K. is funded by Polar Regions and Coasts in the Changing Earth System II (PACES II), the Helmholtz research program to which the Alfred Wegener Institute contributes.

LITERATURE CITED

Abe-Ouchi A, Saito F, Kawamura K, Raymo ME, Okuno JI, et al. 2013. Insolation-driven 100,000-year glacial cycles and hysteresis of ice-sheet volume. *Nature* 500:190–93

Anagnostou E, John EH, Edgar KM, Foster GL, Ridgwell A, et al. 2016. Changing atmospheric CO_2 concentration was the primary driver of early Cenozoic climate. *Nature* 533:380–84

Annan JD, Hargreaves JC. 2013. A new global reconstruction of temperature changes at the Last Glacial Maximum. *Clim. Past* 9:367–76

Arrhenius S. 1896. On the influence of carbonic acid in the air upon the temperature of the ground. *Philos. Mag. Ser.* 5:237–76

Billups K. 2015. Timing is everything during deglaciations. *Nature* 522:163–64

Bloch-Johnson J, Pierrehumbert RT, Abbot DS. 2015. Feedback temperature dependence determines the risk of high warming. *Geophys. Res. Lett.* 42:4973–80

Bony S, Colman R, Kattsov VM, Allan RP, Bretherton CS, et al. 2006. How well do we understand and evaluate climate change feedback processes? *J. Clim.* 19:3445–82

Bony S, Stevens B, Frierson DMW, Jakob C, Kageyama M, et al. 2015. Clouds, circulation and climate sensitivity. *Nat. Geosci.* 8:261–68

Byrne B, Goldblatt C. 2014. Radiative forcing at high concentrations of well-mixed greenhouse gases. *Geophys. Res. Lett.* 41:152–60

Caballero R, Huber M. 2013. State-dependent climate sensitivity in past warm climates and its implications for future climate projections. *PNAS* 110:14162–67

Callendar GS. 1938. The artificial production of carbon dioxide and its influence on temperature. *Q. J. R. Meteorol. Soc.* 64:223–40

Ceppi P, Brient F, Zelinka MD, Hatmann DL. 2017. Cloud feedback mechanisms and their representation in global climate models. *Wiley Interdiscip. Rev. Clim. Change* 8:e465

Charney JG, Arakawa A, Baker DJ, Bolin B, Dickinson RE, et al. 1979. *Carbon Dioxide and Climate: A Scientific Assessment*. Washington, DC: Natl. Acad. Sci.

Cheng H, Edwards RL, Sinha A, Spotl C, Yi L, et al. 2016. The Asian monsoon over the past 640,000 years and ice age terminations. *Nature* 534:640–46

Clark PU, Shakun JD, Marcott SA, Mix AC, Eby M, et al. 2016. Consequences of twenty-first-century policy for multi-millennial climate and sea-level change. *Nat. Clim. Change* 6:360–69

Crowley TJ. 1990. Are there any satisfactory geologic analogs for a future greenhouse warming? *J. Clim.* 3:1282–92

Crucifix M. 2006. Does the Last Glacial Maximum constrain climate sensitivity? *Geophys. Res. Lett.* 33:L24702

DeConto RM, Pollard D. 2003. Rapid Cenozoic glaciation of Antarctica induced by declining atmospheric CO_2. *Nature* 421:245–49

Denton GH, Anderson RF, Toggweiler JR, Edwards RL, Schaefer JM, Putnam AE. 2010. The Last Glacial Termination. *Science* 328:1652–56

Drijfhout S, Bathiany S, Beaulieu C, Brovkin V, Claussen M, et al. 2015. Catalogue of abrupt shifts in Intergovernmental Panel on Climate Change climate models. *PNAS* 112:E5777–86

Dufresne JL, Bony S. 2008. An assessment of the primary sources of spread of global warming estimates from coupled atmosphere-ocean models. *J. Clim.* 21:5135–44

Etminan M, Myhre G, Highwood EJ, Shine KP. 2016. Radiative forcing of carbon dioxide, methane, and nitrous oxide: a significant revision of the methane radiative forcing. *Geophys. Res. Lett.* 43:12614–23

Fasullo JT, Trenberth KE. 2012. A less cloudy future: the role of subtropical subsidence in climate sensitivity. *Science* 338:792–94

Forster PM. 2016. Inference of climate sensitivity from analysis of Earth's energy budget. *Annu. Rev. Earth Planet. Sci.* 44:85–106

Foster GL, Rohling EJ. 2013. Relationship between sea level and climate forcing by CO_2 on geological timescales. *PNAS* 110:1209–14

Friedrich T, Timmermann A, Tigchelaar M, Timm OE, Ganopolski A. 2016. Nonlinear climate sensitivity and its implications for future greenhouse warming. *Sci. Adv.* 2:e1501923

Gasson E, DeConto RM, Pollard D. 2016. Modeling the oxygen isotope composition of the Antarctic ice sheet and its significance to Pliocene sea level. *Geology* 44:827–30

Gleckler PJ, Durack PJ, Stouffer RJ, Johnson GC, Forest CE. 2016. Industrial-era global ocean heat uptake doubles in recent decades. *Nat. Clim. Change* 6:394–96

Grant KM, Rohling EJ, Bar-Matthews M, Ayalon A, Medina-Elizalde M, et al. 2012. Rapid coupling between ice volume and polar temperature over the past 150,000 years. *Nature* 491:744–47

Grant KM, Rohling EJ, Ramsey CB, Cheng H, Edwards RL, et al. 2014. Sea-level variability over five glacial cycles. *Nat. Commun.* 5:5076

Gregory JM, Ingram WJ, Palmer MA, Jones GS, Stott PA, et al. 2004. A new method for diagnosing radiative forcing and climate sensitivity. *Geophys. Res. Lett.* 31:L03205

Hansen J, Kharecha P, Sato M, Masson-Delmotte V, Ackerman F, et al. 2013a. Assessing "dangerous climate change": required reduction of carbon emissions to protect young people, future generations and nature. *PLOS ONE* 8:e81648

Hansen J, Lacis A, Rind D, Russell G, Stone P, et al. 1984. Climate sensitivity: analysis of feedback mechanisms. In *Climate Processes and Climate Sensitivity*, ed. JE Hansen, T Takahashi, pp. 130–63. Washington, DC: Am. Geophys. Union

Hansen J, Ruedy R, Sato M, Lo K. 2010. Global surface temperature change. *Rev. Geophys.* 48:RG4004

Hansen J, Sato M, Kharecha P, Beerling D, Berner R, et al. 2008. Target atmospheric CO_2: Where should humanity aim? *Open Atmos. Sci. J.* 2:217–31

Hansen J, Sato M, Kharecha P, Russell G, Lea DW, Siddall M. 2007. Climate change and trace gases. *Philos. Trans. R. Soc. A* 365:1925–54

Hansen J, Sato M, Kharecha P, von Schuckmann K. 2011. Earth's energy imbalance and implications. *Atmos. Chem. Phys.* 11:13421–49

Hansen J, Sato M, Kharecha P, von Schuckmann K, Beerling DJ, et al. 2017. Young people's burden: requirement of negative CO_2 emissions. *Earth Syst. Dyn.* 8:577–616

Hansen J, Sato M, Ruedy R, Nazarenko L, Lacis A, et al. 2005. Efficacy of climate forcings. *J. Geophys. Res. Atmos.* 110:D18104

Hansen J, Sato M, Russell G, Kharecha P. 2013b. Climate sensitivity, sea level and atmospheric carbon dioxide. *Philos. Trans. R. Soc. A* 371:20120294

Hansen JE, Sato M. 2012. Paleoclimate implications for human-made climate change. In *Climate Change: Inferences from Paleoclimate and Regional Aspects*, ed. A Berger, F Mesinger, D Sijacki, pp. 21–47. Vienna: Springer

Hays JD, Imbrie J, Shackleton NJ. 1976. Variations in earths orbit: pacemaker of ice ages. *Science* 194:1121–32

Hegerl GC, Crowley TJ, Hyde WT, Frame DJ. 2006. Climate sensitivity constrained by temperature reconstructions over the past seven centuries. *Nature* 440:1029–32

Hoffman JS, Clark PU, Parnell AC, He F. 2017. Regional and global sea-surface temperatures during the last interglaciation. *Science* 355:276–79

Holloway MD, Sime LC, Singarayer JS, Tindall JC, Bunch P, Valdes PJ. 2016. Antarctic last interglacial isotope peak in response to sea ice retreat not ice-sheet collapse. *Nat. Commun.* 7:12293

IPCC (Intergov. Panel Clim. Change). 2013. *Climate Change 2013: The Physical Science Basis. Contribution of Working Group I to the Fifth Assessment Report of the Intergovernmental Panel on Climate Change*. Cambridge, UK: Cambridge Univ. Press

Kemp DB, Eichenseer K, Kiessling W. 2015. Maximum rates of climate change are systematically underestimated in the geological record. *Nat. Commun.* 6:8890

Kirschvink JL. 1992. Late proterozoic low latitude global glaciation: the snowball Earth. In *The Proterozoic Biosphere: A Multidisciplinary Study*, ed. JW Schoff, C Klein, pp. 51–52. New York: Cambridge Univ. Press
Knutti R, Hegerl GC. 2008. The equilibrium sensitivity of the Earth's temperature to radiation changes. *Nat. Geosci.* 1:735–43
Knutti R, Rugenstein MAA. 2015. Feedbacks, climate sensitivity and the limits of linear models. *Philos. Trans. R. Soc. Lond. A* 373:20150146
Köhler P, Bintanja R, Fischer H, Joos F, Knutti R, et al. 2010. What caused Earth's temperature variations during the last 800,000 years? Data-based evidence on radiative forcing and constraints on climate sensitivity. *Quat. Sci. Rev.* 29:129–45
Köhler P, de Boer B, von der Heydt AS, Stap LB, van de Wal R. 2015. On the state dependency of the equilibrium climate sensitivity during the last 5 million years. *Clim. Past* 11:1801–23
Lambeck K, Rouby H, Purcell A, Sun Y, Sambridge M. 2014. Sea level and global ice volumes from the Last Glacial Maximum to the Holocene. *PNAS* 111:15296–303
Lord NS, Ridgwell A, Thorne MC, Lunt DJ. 2016. An impulse response function for the "long tail" of excess atmospheric CO_2 in an Earth system model. *Glob. Biogeochem. Cycles* 30:2–17
Lunt DJ, Haywood AM, Schmidt GA, Salzmann U, Valdes PJ, Dowsett HJ. 2010. Earth system sensitivity inferred from Pliocene modelling and data. *Nat. Geosci.* 3:60–64
Mann ME. 2014. False hope. *Sci. Am.* 310:78–81
Marcott SA, Bauska TK, Buizert C, Steig EJ, Rosen JL, et al. 2014. Centennial-scale changes in the global carbon cycle during the last deglaciation. *Nature* 514:616–19
MARGO. 2009. Constraints on the magnitude and patterns of ocean cooling at the Last Glacial Maximum. *Nat. Geosci.* 2:127–32
Marino G, Rohling EJ, Rodriguez-Sanz L, Grant KM, Heslop D, et al. 2015. Bipolar seesaw control on last interglacial sea level. *Nature* 522:197–201
Martínez-Botí MA, Foster GL, Chalk TB, Rohling EJ, Sexton PF, et al. 2015. Plio-Pleistocene climate sensitivity evaluated using high-resolution CO_2 records. *Nature* 518:49–54
Marvel K, Schmidt GA, Miller RL, Nazarenko LS. 2016. Implications for climate sensitivity from the response to individual forcings. *Nat. Clim. Change* 6:386–89
Masson-Delmotte V, Buiron D, Ekaykin A, Frezzotti M, Gallee H, et al. 2011. A comparison of the present and last interglacial periods in six Antarctic ice cores. *Clim. Past* 7:397–423
Masson-Delmotte V, Stenni B, Pol K, Braconnot P, Cattani O, et al. 2010. EPICA Dome C record of glacial and interglacial intensities. *Quat. Sci. Rev.* 29:113–28
Myhre G, Highwood EJ, Shine KP, Stordal F. 1998. New estimates of radiative forcing due to well mixed greenhouse gases. *Geophys. Res. Lett.* 25:2715–18
Myhre G, Shindell D, Bréon F-M, Collins W, Fuglestvedt J, et al. 2013. Anthropogenic and natural radiative forcing. In *Climate Change 2013: The Physical Science Basis. Contribution of Working Group I to the Fifth Assessment Report of the Intergovernmental Panel on Climate Change*, ed. TF Stocker, D Qin, G-K Plattner, M Tignor, SK Allen, et al, pp. 659–740. Cambridge, UK: Cambridge Univ. Press
Pagani M, Liu ZH, LaRiviere J, Ravelo AC. 2010. High Earth-system climate sensitivity determined from Pliocene carbon dioxide concentrations. *Nat. Geosci.* 3:27–30
PALAEOSENS. 2012. Making sense of palaeoclimate sensitivity. *Nature* 491:683–91
Poulsen CJ, Jacob RL, Pierrehumbert RT, Huynh TT. 2002. Testing paleogeographic controls on a Neoproterozoic snowball Earth. *Geophys. Res. Lett.* 29:10-1–4
Proistosescu C, Huybers PJ. 2017. Slow climate mode reconciles historical and model-based estimates of climate sensitivity. *Sci. Adv.* 3:e1602821
Rohling EJ, Grant K, Bolshaw M, Roberts AP, Siddall M, et al. 2009. Antarctic temperature and global sea level closely coupled over the past five glacial cycles. *Nat. Geosci.* 2:500–4
Rohling EJ, Haigh ID, Foster GL, Roberts AP, Grant KM. 2013. A geological perspective on potential future sea-level rise. *Sci. Rep.* 3:3461
Rohling EJ, Medina-Elizalde M, Shepherd JG, Siddall M, Stanford JD. 2012. Sea surface and high-latitude temperature sensitivity to radiative forcing of climate over several glacial cycles. *J. Clim.* 25:1635–56
Rose BEJ, Rayborn L. 2016. The effects of ocean heat uptake on transient climate sensitivity. *Curr. Clim. Change Rep.* 2:190–201

Royer DL. 2016. Climate sensitivity in the geologic past. *Annu. Rev. Earth Planet. Sci.* 44:277–93
Rugenstein MAA, Caldeira K, Knutti R. 2016a. Dependence of global radiative feedbacks on evolving patterns of surface heat fluxes. *Geophys. Res. Lett.* 43:9877–85
Rugenstein MAA, Gregory JM, Schaller N, Sedlacek J, Knutti R. 2016b. Multiannual ocean-atmosphere adjustments to radiative forcing. *J. Clim.* 29:5643–59
Schmidt GA, Severinghaus J, Abe-Ouchi A, Alley RB, Broecker W, et al. 2017. Overestimate of committed warming. *Nature* 547:E16–17
Schmittner A, Urban NM, Shakun JD, Mahowald NM, Clark PU, et al. 2011. Climate sensitivity estimated from temperature reconstructions of the Last Glacial Maximum. *Science* 334:1385–88
Schneider von Deimling T, Held H, Ganopolski A, Rahmstorf S. 2006. Climate sensitivity estimated from ensemble simulations of glacial climate. *Clim. Dyn.* 27:149–63
Shackleton NJ. 2000. The 100,000-year ice-age cycle identified and found to lag temperature, carbon dioxide, and orbital eccentricity. *Science* 289:1897–902
Shakun JD, Clark PU, He F, Marcott SA, Mix AC, et al. 2012. Global warming preceded by increasing carbon dioxide concentrations during the last deglaciation. *Nature* 484:49–54
Sherwood SC, Bony S, Dufresne JL. 2014. Spread in model climate sensitivity traced to atmospheric convective mixing. *Nature* 505:37–42
Skinner L. 2012. A long view on climate sensitivity. *Science* 337:917–19
Snyder CW. 2016. Evolution of global temperature over the past two million years. *Nature* 538:226–28
Stevens B, Sherwood SC, Bony S, Webb MJ. 2016. Prospects for narrowing bounds on Earth's equilibrium climate sensitivity. *Earth's Future* 4:512–22
Stocker TF. 1998. The seesaw effect. *Science* 282:61–62
Stocker TF, Johnsen SJ. 2003. A minimum thermodynamic model for the bipolar seesaw. *Paleoceanography* 18:1087
Storelvmo T, Leirvik T, Lohmann U, Phillips PCB, Wild M. 2016. Disentangling greenhouse warming and aerosol cooling to reveal Earth's climate sensitivity. *Nat. Geosci.* 9:286–89
Tzedakis PC, Crucifix M, Mitsui T, Wolff EW. 2017. A simple rule to determine which insolation cycles lead to interglacials. *Nature* 542:427–32
van de Wal RSW, de Boer B, Lourens LJ, Köhler P, Bintanja R. 2011. Reconstruction of a continuous high-resolution CO_2 record over the past 20 million years. *Clim. Past* 7:1459–69
Vial J, Dufresne JL, Bony S. 2013. On the interpretation of inter-model spread in CMIP5 climate sensitivity estimates. *Clim. Dyn.* 41:3339–62
von der Heydt AS, Ashwin P. 2016. State dependence of climate sensitivity: attractor constraints and palaeoclimate regimes. *Dyn. Stat. Clim. Syst.* 1:dzx001
von der Heydt AS, Dijkstra HA, van de Wal RSW, Caballero R, Crucifix M, et al. 2016. Lessons on climate sensitivity from past climate changes. *Curr. Clim. Change Rep.* 2:148–58
von der Heydt AS, Köhler P, van de Wal RSW, Dijkstra HA. 2014. On the state dependency of fast feedback processes in (paleo) climate sensitivity. *Geophys. Res. Lett.* 41:6484–92
Whitmarsh F, Zika J, Czaja A. 2015. *Ocean heat uptake and the global surface temperature record*. Grantham Inst. Brief. Pap. 14, Grantham Inst., Imperial Coll. Lond. **https://www.imperial.ac.uk/media/imperial-college/grantham-institute/public/publications/briefing-papers/Ocean-heat-uptake—Grantham-BP-15.pdf**
Zachos JC, Schouten S, Bohaty S, Quattlebaum T, Sluijs A, et al. 2006. Extreme warming of mid-latitude coastal ocean during the Paleocene-Eocene Thermal Maximum: inferences from TEX86 and isotope data. *Geology* 34:737–40
Zeebe RE. 2013. Time-dependent climate sensitivity and the legacy of anthropogenic greenhouse gas emissions. *PNAS* 110:13739–44
Zeebe RE, Ridgwell A, Zachos JC. 2016. Anthropogenic carbon release rate unprecedented during the past 66 million years. *Nat. Geosci.* 9:325–29
Zeebe RE, Zachos JC, Dickens GR. 2009. Carbon dioxide forcing alone insufficient to explain Palaeocene-Eocene Thermal Maximum warming. *Nat. Geosci.* 2:576–80
Zhou C, Zelinka MD, Klein SA. 2016. Impact of decadal cloud variations on the Earth's energy budget. *Nat. Geosci.* 9:871–74

Annual Review of Marine Science

Volume 10, 2018

Contents

Errata

An online log of corrections to *Annual Review of Marine Science* articles may be found at http://www.annualreviews.org/errata/marine